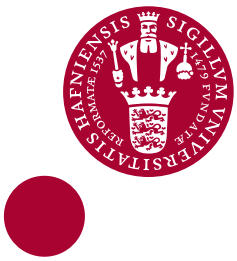

Depostitional Evolution of the Western Amundsen Basin, Arctic Ocean Paleoceangraphic and Tectonic Implication

Castro, Carlos F.; Knutz, Paul C.; Hopper, John R.; Funck, Thomas

Published in:
Paleoceanography

DOI:
10.1029/2018PA003414

Publication date:
2018

Document version
Publisher's PDF, also known as Version of record

Paleoceanography and Paleoclimatology

RESEARCH ARTICLE
10.1029/2018PA003414

Key Points:
- New multichannel seismic reflection data constrain the Cenozoic depositional history of the Amundsen Basin in the Arctic Ocean
- Four key development stages explain the basin evolution based on facies interpretation and estimated sedimentation rates
- Plio-Pleistocene cascading plumes, possibly from brine formation, affected the North Greenland shelf and influenced deep circulation

Supporting Information:
- Supporting Information S1

Correspondence to:
C. F. Castro,
cfc@geus.dk

Citation:
Castro, C. F., Knutz, P. C., Hopper, J. R., & Funck, T. (2018). Depositional evolution of the western Amundsen Basin, Arctic Ocean: Paleoceanographic and tectonic implications. *Paleoceanography and Paleoclimatology*, *33*, 1357–1382. https://doi.org/10.1029/2018PA003414

Received 5 JUN 2018
Accepted 1 OCT 2018
Accepted article online 5 OCT 2018
Published online 12 DEC 2018

Depositional Evolution of the Western Amundsen Basin, Arctic Ocean: Paleoceanographic and Tectonic Implications

Carlos F. Castro[1,2], Paul C. Knutz[1], John R. Hopper[1], and Thomas Funck[1]

[1]Geological Survey of Denmark and Greenland, Copenhagen K, Denmark, [2]Niels Bohr Institute, University of Copenhagen, Copenhagen, Denmark

Abstract A new stratigraphic model and estimated sedimentation rates of the western Amundsen Basin, Arctic Ocean, are presented based on multichannel seismic reflection data, seismic refraction data, magnetic data, and integrated with the sedimentary sequence from the central Arctic Ocean, obtained during the Arctic Coring Expedition. This places new constraints on the postbreakup Cenozoic depositional history of the basin, the adjacent Lomonosov Ridge, and improves the understanding of the tectonic, climatic, and oceanographic conditions in the central Arctic region. Four distinct phases of basin development are proposed. During the Paleocene-mid-Oligocene, high sedimentation rates are linked to terrestrial input and increased pelagic deposition in a restricted basin. Deposition of sedimentary wedges and mass transport into marginal depocenters reflect a period of tectonic instability linked to compression associated with the Eurekan Orogeny in the Arctic. During the late Oligocene-early Miocene, widespread passive infill associated with hemipelagic deposition reflects a phase of limited tectonism, most likely in a freshwater estuarine setting. During the middle Miocene, mounded sedimentary buildups along the Lomonosov Ridge suggest the onset of geostrophic bottom currents that likely formed in response to a deepening and widening of the Fram Strait beginning around 18 Ma. In contrast, the Plio-Pleistocene stage is characterized by erosional features such as scarps and channels adjacent to levee accumulations, indicative of a change to a higher-energy environment. These deposits are suggested to be partly associated with dense shelf water-mass plumes driven by supercooling and brine formation over the northern Greenland continental shelf.

1. Introduction

The Cenozoic development of the Amundsen Basin (Figure 1) and its role in the paleoceanographic evolution of the Arctic Ocean remains poorly understood. This lack of knowledge is due in part to the challenges of acquiring data in areas with perennial sea ice cover. Only few seismic profiles have been acquired in the region, and these are unconstrained by stratigraphic control. Seismic reflection data were mostly collected with short streamers and small source arrays. Seismic refraction data were collected with sonobuoys and, in some instances, recoverable ice stations (e.g., Chernykh & Krylov, 2011; Fütterer, 1992; Jokat et al., 1995a; Jokat & Micksch, 2004; Ostenso & Wold, 1977). Rock samples collected by dredging are sparse (Brumley et al., 2015; Knudsen et al., 2017; Michael et al., 2003) and shallow cores (Fütterer, 1992; Svindland & Vorren, 2002) constrain only the most recent Quaternary depositional history. The only source of deep stratigraphic information comes from scientific ocean drilling during Integrated Ocean Drilling Program expedition 302, the Arctic Coring Expedition (ACEX). During ACEX, samples were recovered on the central Lomonosov Ridge (LR) in 2004 to a depth of ~400 m (Backman et al., 2005). Much of the tectono-oceanographic history of the Amundsen Basin and the adjacent LR remains unknown.

The objective of this paper is to investigate the Cenozoic depositional history of the Amundsen Basin using new multichannel seismic reflection data gathered as part of the United Nations Convention on the Law of the Sea program for the continental shelf project of the Kingdom of Denmark. The lines were collected in the western part of the Amundsen Basin and along the flank of the Eurasian side of the LR (Figure 1). The data are supplemented by published multichannel seismic data in the Amundsen Basin (Jokat et al., 1995a, 1995b; Jokat & Micksch, 2004), magnetic data (Brozena et al., 2003), and information from ACEX drill sites (Jakobsson et al., 2007; Moran et al., 2006). Linking these data sets offers the opportunity to advance previous stratigraphic interpretations in the Amundsen Basin (e.g., Chernykh & Krylov, 2011; Jokat et al., 1995a) and

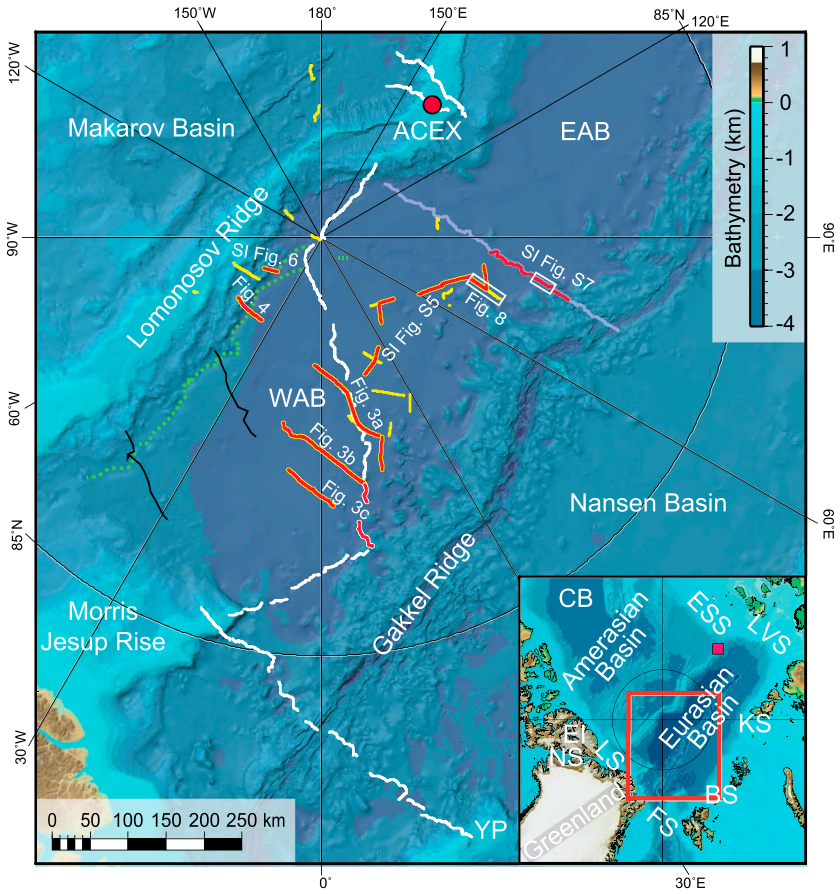

Figure 1. Bathymetry of the Amundsen Basin and surrounding areas in the Arctic Ocean. (yellow lines) LOMROG multichannel seismic reflection data collected in 2007, 2009, and 2012. (white lines) Seismic reflection data from ARCTIC'91 (Jokat et al., 1995a, 1995b). (purple line) Seismic reflection data from AMORE 2001 (Jokat & Micksch, 2004). (black lines) Seismic reflection lines from NP-28 (Fütterer, 1992) and Arlis-II (Ostenso & Wold, 1977). (red lines and white rectangles) Seismic reflection segments featured in this paper. (green lines) Major sediment pathways from Boggild and Mosher (2016). (red-filled circle) Location of Integrated Ocean Drilling Program 302 (ACEX). (red-filled square) Location of coring station from PS87/2014 (Stein et al., 2016). The bathymetry is based on the IBCAO grid v.3 (Jakobsson et al., 2012). BS = Barents shelf; CB = Canada Basin; ESS = East Siberian Shelf; EAB = Eastern Amundsen Basin; EI = Ellesmere Island; FS = Fram Strait; KS = Kara Shelf; LVS = Laptev Shelf; LS = Lincoln Shelf; NS = Nares Strait; RU = Russia; SAT = St. Anna Trough; WAB = Western Amundsen Basin; YP = Yermak Plateau; ACEX = Arctic Coring Expedition.

improve our understanding of the sedimentary processes and tectonic evolution of the Arctic Ocean. Moreover, the continuous basin record may also supplement the incomplete ACEX record and provide additional constraints on the missing history of the LR. In this contribution, a new stratigraphic model of the Amundsen Basin is presented, and four main evolutionary stages are proposed.

2. Geological and Oceanographic Setting

The LR is a sliver of continental crust that connects the Lincoln Shelf north of Greenland and Ellesmere Island to the East Siberian Shelf, separating the Arctic Ocean into two main basins—the Amerasian Basin and Eurasian Basin (Figure 1). The Eurasian Basin is bisected by the world's slowest mid-ocean ridge spreading center, with present day full spreading rates of 14.6 mm/year at the western end, decreasing to 6.3 mm/year in the Laptev Sea (DeMets et al., 1994). It is generally agreed that seafloor spreading began in the early Cenozoic as the LR rifted away from the Barents and Kara shelves when Greenland and North America separated from Eurasia (Jokat et al., 1992; Poselov et al., 2014; Talwani & Eldholm, 1977; Vogt et al., 1979). Magnetic anomalies indicate that spreading began no later than Chron C24N (~53 Ma, the timescale of Ogg, 2012, is used throughout this paper) and possibly during Chron C25 (~57 Ma; Brozena et al., 2003; Cochran et al.,

2006; Døssing, Hopper, et al., 2013; Døssing, Jackson, et al., 2013; Engen et al., 2008; Glebovsky et al., 2006; Vogt et al., 1979).

The LR was first proposed as a continental fragment by Heezen and Ewing (1961). This was confirmed subsequently by seismic data (Ostenso & Wold, 1977; Sweeney et al., 1982). Seismic profiles across the LR show structures below cover dominated by crustal scale extension. Tilted continental fault blocks are well imaged and continuous with horst and graben-like bathymetry toward Siberia (Jokat, 2005; Jokat et al., 1992). The oldest sedimentary rocks recovered by the ACEX drilling leg are Late Cretaceous age (i.e., prebreakup; Backman et al., 2005). Metamorphic sandstones recovered by dredging the Eurasian flank of the ridge have a Mid-Ordovician deformation age, showing that the LR was involved in a collisional event at that time (Knudsen et al., 2017). The combined evidence unequivocally demonstrates the continental nature of the ridge.

Another discovery of the ACEX expedition was the presence of a depositional hiatus spanning from the mid-Eocene-early Miocene (Moran et al., 2006) based on biostratigraphic data (Backman et al., 2008). This hiatus is unexpected because it is inconsistent with established postrift thermal subsidence models (McKenzie, 1978). O'Regan et al. (2008) suggested that the ridge remained at or near sea level during the duration of the time gap. Based on an analysis of the consolidation, strength, and permeability of the sediments recovered, O'Regan et al. (2010) suggest that the hiatus arose from a period of prolonged low to nondeposition. The cause of nondeposition and/or erosion has been attributed to tectonic uplift, either as a result of mantle phase changes (Minakov & Podladchikov, 2012) or as a result of the Eurekan orogeny, which reached its peak during the Eocene (Døssing et al., 2014). Others have related the hiatus to erosion by oceanic bottom currents (Jokat et al., 1992; Moore and the Expedition 302 Scientists, 2006a), implying that a vigorous circulation system was established in the late Eocene, although this may have happened in combination with tectonic uplift (O'Regan et al., 2008).

An alternative chronology to the 26-Ma hiatus model by Backman et al. (2008) was derived from Re-Os isotope data produced by Poirier and Hillaire-Marcel (2009, 2011), who proposed that middle Cenozoic sedimentation rates on the LR were continuous (albeit ultraslow) with a time gap of $<$0.4 Ma at about 36 Ma. The two different age models have drastically different implications for the timing of a fully ventilated Arctic Ocean and for the tectonic evolution of the LR (O'Regan et al., 2011; Stein et al., 2014). In the original Backman et al. (2008) model (hereafter referred to as age model 1), the LR is linked to a period of delayed subsidence, and the transition from a lake to a marine setting is placed at approximately 17.5 Ma (Jakobsson et al., 2007). In the second model by Poirier and Hillaire-Marcel (2009, 2011; hereafter referred to as age model 2), the onset of marine conditions in the Arctic is inferred at approximately 36 Ma, suggesting instead that the LR experienced a gradual change in relative sea level during the Oligocene-Miocene. Throughout the paper, when discussing timing and ages with respect to specific features and interpretations, we refer to age model 1, since it is well established in the literature. The implications for age model 2 are discussed separately in a subsection of the discussion.

Weigelt et al. (2014) summarized previous stratigraphic interpretations of the Arctic Ocean and proposed a new scheme based primarily on data from the Siberian Shelf and Laptev Sea. Currently, there are two principal stratigraphic schemes for the western Amundsen Basin (WAB), with very different implications for sedimentation rates and oceanographic settings. Jokat et al. (1995a) suggest that prior to polarity Chron C13N (~34 Ma), sedimentation rates throughout the basin were uniformly high, varying from 10 to 15 cm/ka. Since that time, sedimentation rates have decreased to 1.5 cm/ka. Alternatively, Chernykh and Krylov (2011) suggest that the average sedimentation rates have gradually decreased from about 30 to $<$4 cm/ka from the onset of spreading until the late Oligocene (Chattian, approximately 28–23 Ma), after which sedimentation rates sharply increased to about 10 cm/ka due to a global marine regression, and then later decreased to $<$2 cm/ka during the Miocene. These different models have important implications for understanding the paleoceanographic environment of the Arctic Ocean.

The Arctic Ocean serves two key roles in the ocean circulation system: (1) it provides a passage between the Atlantic and Pacific oceans; and (2) it provides a receptacle for Atlantic water masses, alters them, and then returns them back to the Atlantic (Rudels & Friedrich, 2000). The Atlantic water inflow, primarily via the Fram Strait and the St. Anna Trough in the Barents Sea, is mainly driven by thermohaline circulation (Beszczynska-Möller et al., 2011). The Atlantic water current system, termed the Atlantic Ocean boundary current, is a

Table 1
Summary of Key Acquisition Parameters During LOMROG I Through III

	LOMROG I	LOMROG II	LOMROG III
Source	1 Sercel G and 1 Sercel GI gun	1 Sercel G and 1 Sercel GI gun	2*Sercel G-Gun
Chamber volume (inch^3)	605	605	1,040
Gun pressure	200 bar (3,000 psi)	180 bar (2,600 psi)	180 bar (2,600 psi)
Nominal tow depth (m)	20	20	20
Streamer	Geometrics GeoEel	Geometrics GeoEel	Geometrics GeoEel
Length of tow cable (m)	43	43	30
Total no. of groups	48/40/32/24	32/40	32
Group interval (m)	6.25	6.25	6.25
Nominal tow depth (m)	20	20	20

Note. The data quality was enhanced by a basic processing sequence that included band pass filtering, spectral shaping filtering, spike and noise burst editing, f-k filtering, static corrections, trace equalization, shot-mixing, stacking, and velocity migrations.

subsurface water mass (depths between about 150 and 900 m) that flows in a cyclonic (anticlockwise) direction following the topographic basin slopes and along the ocean ridges (Rudels, 1995, 2012; Tomczak & Godfrey, 1994; Woodgate, 2013). In contrast, the uppermost waters are wind-driven and flow anticyclonically in the Beaufort Gyre in the southern Canada Basin, where it contributes to the transpolar sea-ice drift from Siberia toward the Fram Strait (Rudels, 2012). Despite the present understanding of Arctic oceanography, little is known about deep ocean currents formed in the region, their role in sediment transportation and deposition, and possible influence on the global meridional overturn circulation.

3. Seismic Database

The seismic data used in this study consist of several recent and vintage surveys acquired along the central Amundsen Basin and the flanks of the LR within a region of very sparse coverage of multichannel seismic reflection data. The database consists primarily of 2-D-reflection data from several marine seismic expeditions collected for the United Nations Convention on the Law of the Sea program of the Kingdom of Denmark, described briefly below and in more detail in supporting information S1. In addition, seismic lines from two older surveys were used (Figure 1): ARCTIC'91 (~1,500 km) and AMORE 2001 (550 km; Jokat et al., 1995a, 1995b; Jokat & Micksch, 2004).

The LOMROG surveys were acquired in 2007, 2009, and 2012 using a high-resolution seismic system designed for use in Arctic sea ice and was deployed from the Swedish icebreaker *Oden* (Hopper et al., 2012). Key acquisition parameters are summarized in Table 1. Details from each survey are provided in Marcussen et al. (2008), Lykke-Andersen et al. (2010), and Varming et al. (2012). The source array consisted of G and G-I guns with various configurations and a streamer of up to 300 m long with a group interval of 6.25 m. The nominal towing depth of both the source and receiver arrays was set to 20 m to minimize interference with ice. Further acquisition and processing details are provided in supporting information S1.

The seismic refraction data were obtained by sonobuoys, which recorded the shots from the seismic reflection experiments. In this study, four sonobuoys were used for constraining sediment velocities in the Amundsen Basin (Figure 2). The velocity modeling and sonobuoy data are presented in Figures S1–S4. The seismic energy produced by the airgun cluster could be recorded up to offsets of 20 km. *P* wave velocity models of the sediments and the underlying crust were then obtained by forward modeling of the travel times using RAYINVR software based on the algorithm of Zelt and Smith (1992). The coincident seismic reflection data were used to guide the velocity modeling down to the basement.

4. Description and Timing of Main Seismic Units

The key seismic units were identified based on reflection character, seismic facies, and geometries (Mitchum et al., 1977). Ages for the top of the older units were derived by establishing the point where seismic horizons onlap the basement and then infer basement ages from the magnetic anomaly interpretation of Brozena

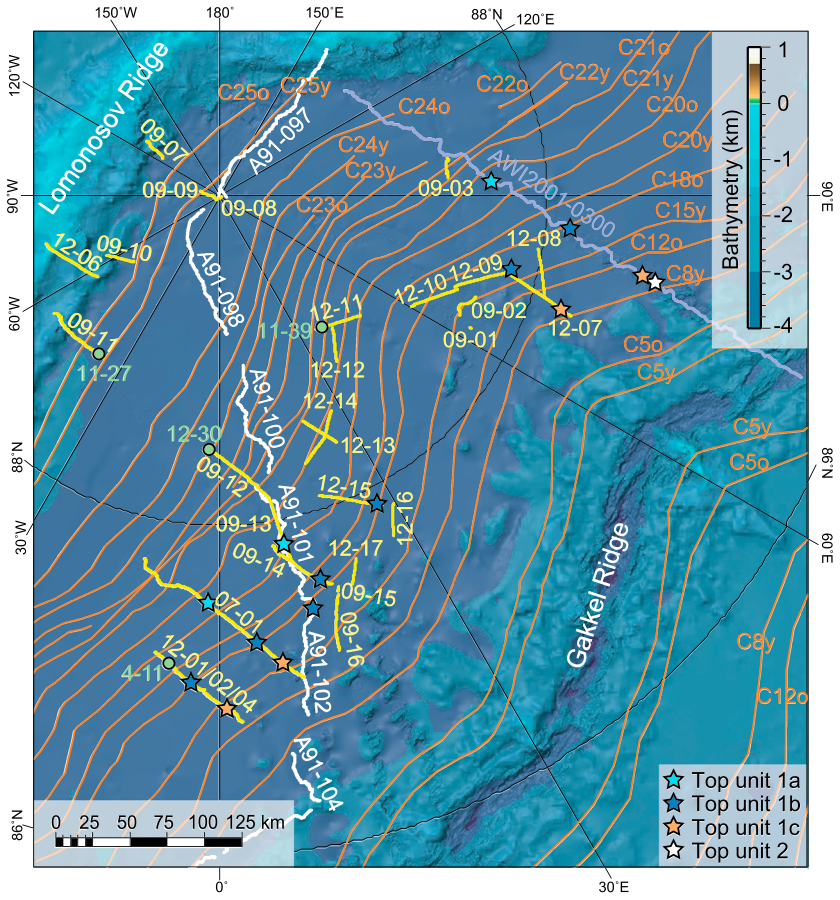

Figure 2. Magnetic anomaly map from Brozena et al. (2003) used to determine the ages of the stratigraphic units in this study. (orange lines) Normal polarity chrons. The "y" and "o" refer to the young and old side of the anomalies, respectively. (yellow lines) LOMROG multichannel seismic reflection data collected in 2007, 2009, and 2012. The seismic lines are labeled "xx-yy", where "xx" refers to the year the data were collected, and "yy" refers to the profile number. (white lines) Seismic reflection data from ARCTIC'91 (Jokat et al., 1995a). The seismic lines are labeled "A91-yyy", where "A91" refers to "AWI1991," and "yyy" refers to the profile number. (purple line) Seismic reflection data from AMORE 2001 (Jokat & Micksch, 2004). (light blue-filled stars) Position where the top horizon of subunit 1a onlaps the oceanic basement. (dark blue-filled stars) Position where the top horizon of subunit 1b onlaps the oceanic basement. (orange-filled stars) Position where the top horizon of subunit 1c onlaps the oceanic basement. (white-filled star) Position where the top horizon of unit 2 onlaps the oceanic basement. (green-filled circles) Deployment position of sonobuoys used in this study.

et al. (2003) recalibrated to the timescale of Ogg (2012). This provides a maximum age for a horizon since the sediments must be younger than the underlying oceanic crust. The thicknesses of the units were derived from the two-way travel time in the seismic reflection data and from the velocities obtained from the refraction data. For each unit, a range of sedimentation rates (min/max) was calculated based on sediment thickness variations between individual basin segments (e.g., between structural highs) and the correlation of key horizons to the magnetic time scale as expressed on the seafloor.

4.1. Seismic Stratigraphy

The sediments within the WAB are dominated by parallel strata forming a uniform and continuous drape over the oceanic basement, which has a highly variable relief and in some places protrudes above the otherwise flat and uniform basin floor. The WAB succession is divided into six seismic units, each bounded by reflections that are generally conformable but clearly demarcate changes in seismic facies. The thickest unit, unit 1, was further subdivided based on facies changes or locally developed internal reflections.

Figure 3 shows a summary overview of long transects through the basin running perpendicular to the strike of the Lomonosov and Gakkel ridges. A similar transect running parallel to the ridges through the central part

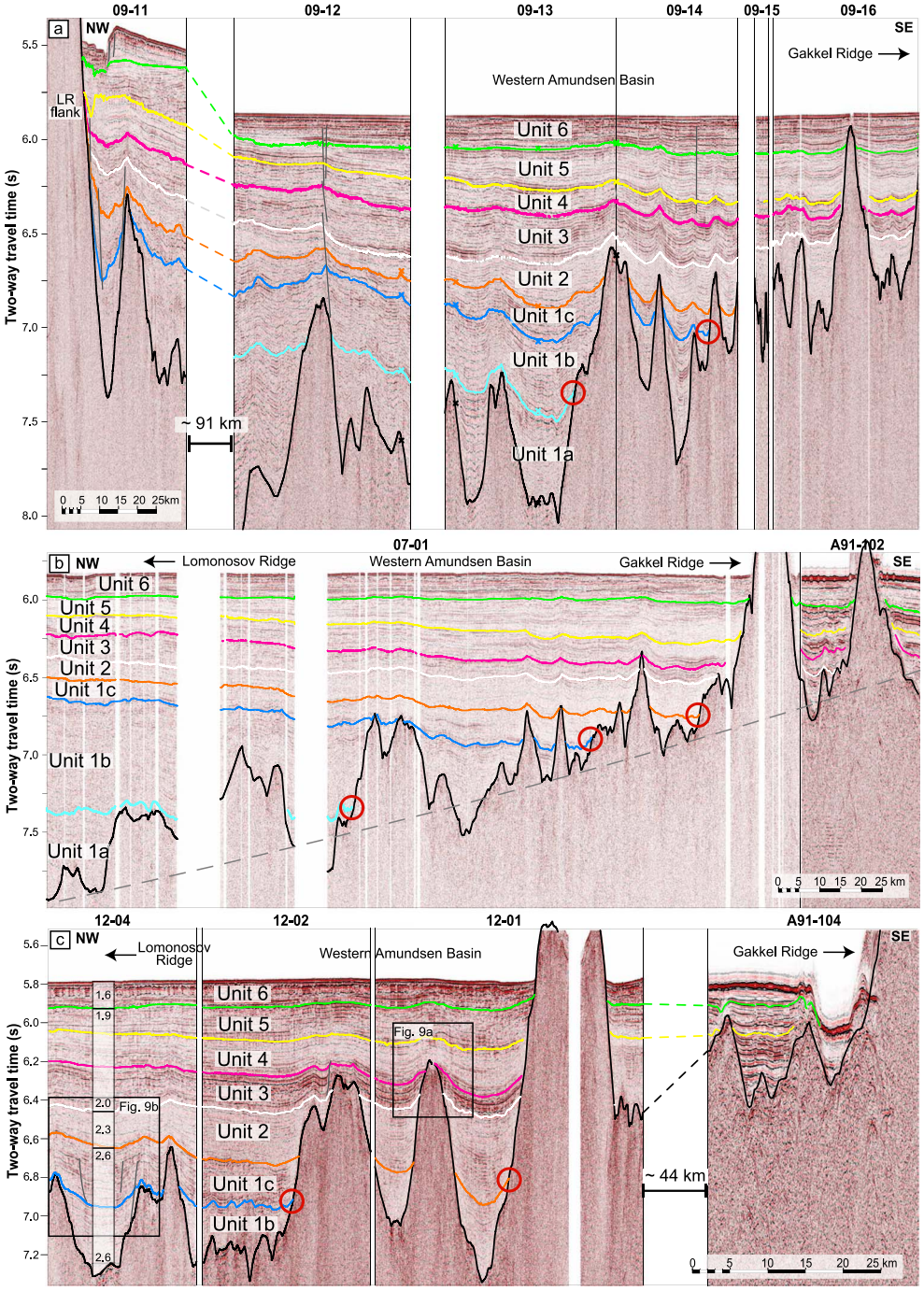

Figure 3. Three seismic transects crossing the Amundsen Basin with line names shown along the top axis (see Figures 1 and 2 for line positions). Key seismic horizons interpreted: oceanic basement = black; top subunit 1a = light blue (C21y–C20o, 44.5 ± 1.5 Ma); top subunit 1b = dark blue (C18o–C15y, 37.5 ± 2.5 Ma); top subunit 1c = orange (C18y–C12o, 27.5 ± 2.5 Ma); top subunit 2 = white (<C8y, < 25–20 Ma); top unit 3 = magenta; top unit 4 = yellow; top unit 5 = green; top unit 6 = seabed. (red circles) Positions where the horizons onlap the oceanic basement (see Figure 2). (gray-dashed line) Estimated thermal subsidence curve of the seafloor according to plate cooling models (Parsons & Sclater, 1977). y = young; o = old.

of the basin is shown in Figure S5. Detailed seismic sections crossing the flank of the LR into the WAB are shown in Figures 3–7 and S6, while detailed sections of the stratigraphy in the central parts of the basin are shown in Figures 8, 9 and S7.

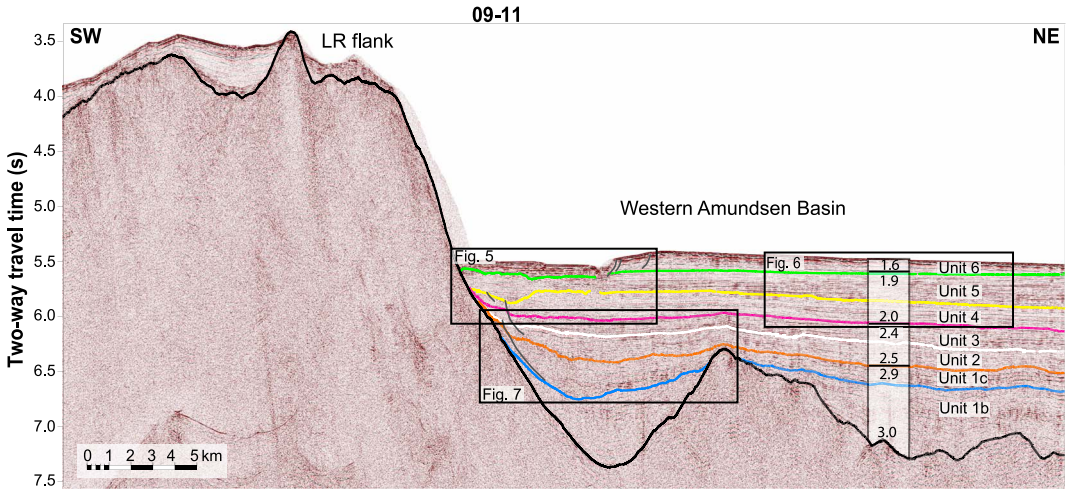

Figure 4. Seismic profile LOMROG2009-11 crossing the LR flank into the Amundsen Basin. Key seismic horizons interpreted: oceanic basement = black; top subunit 1b = dark blue (C18o–C15y, 37.5 ± 2.5 Ma); top subunit 1c = orange (C18y–C12o, 27.5 ± 2.5 Ma); top subunit 2 = white (<C8y, < 25–20 Ma); top unit 3 = magenta; top unit 4 = yellow; top unit 5 = green; top unit 6 = seabed. A 1-D-velocity column modeled from the refraction data is shown. LR= Lomonosov Ridge; y = young; o = old.

4.1.1. Unit 1

The lowermost unit is the thickest unit in the basin, with a maximum thickness of about 1,450 ms (~2,150 m). The base of the unit is marked by the top of the igneous oceanic crust, which shows significant relief and often appears to be faulted. Throughout the rest of this paper, basement refers to the top oceanic crust. Unit 1 is the thickest in the oldest part of the basin and thins toward the Gakkel Ridge. In the central WAB, the unit is often confined by the uneven topography and fills isolated subbasins (Figure 3a). At the LR flank, the thickness of unit 1 ranges from about 700 to 1,000 ms (~1,000 to 1,450 m; Figures 3 and 4).

The unit can be subdivided into three subunits (Figures 3a and 3b). The lower subunit, 1a, consists of variable internal reflections, ranging from weak or poorly defined to strong and continuous (Figures 3a and 3b). It is not observed in areas where the basement shallows. The middle subunit, 1b, consists of predominantly weak

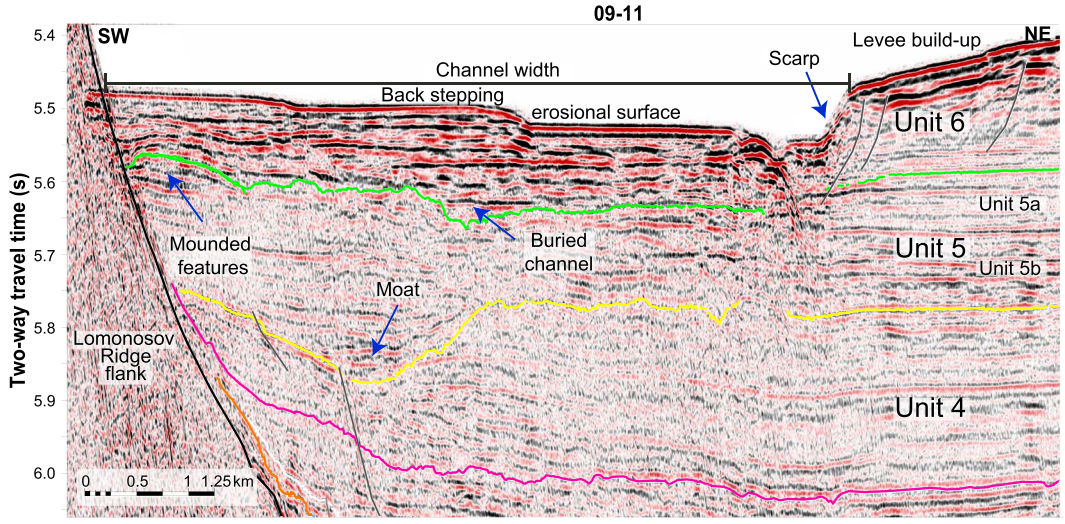

Figure 5. Detail of channel segment developed within unit 6 (see position in Figure 4). The channel system is characterized by terraced surfaces back-stepping toward the ridge flank. Note the prominent development of the basinward channel levee influenced by growth faults and asymmetric mounded depositional features seen within units 4 and 5. Unit 5 is divided into two subunits (a and b). Key seismic horizons interpreted: oceanic basement = black; top subunit 1c = orange (C18y–C12o, 27.5 ± 2.5 Ma); top subunit 2 = white (<C8y, <25–20 Ma); top unit 3 = magenta; top unit 4 = yellow; top unit 5 = green; top unit 6 = seabed. y = young; o = old.

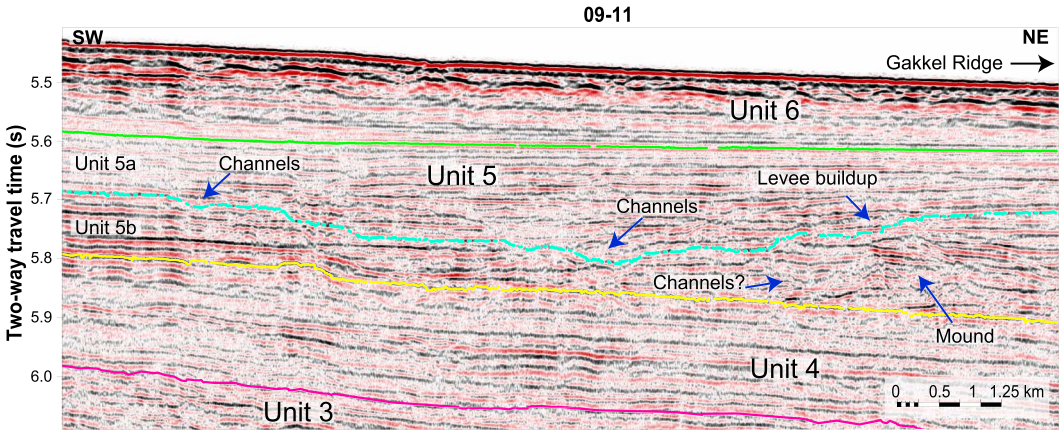

Figure 6. Detail from Figure 4 showing erosion within unit 5 interpreted as a buried channel segment (turquoise dot-dash horizon). The buried channel is about 7 km wide and shows a stepwise incision with a preferential levee accumulation in a basinward direction similar to the modern channel. Key seismic horizons interpreted: top unit 3 = magenta; top unit 4 = yellow; top unit 5 = green; top unit 6 = seabed.

reflections and is often transparent (Figures 3a–3c). The thickness of subunit 1b is typically about 400 ms (~500 m); however, in profile 07-01 across the central Amundsen Basin, it reaches up to 700 ms (~900 m; Figure 3b). The upper subunit, 1c, is marked by semicontinuous relatively coherent reflections. The seismic geometries are strongly influenced by basement relief and within the thickest sections internal discontinuities are common (Figure 3c). The thickness of subunit 1c ranges from about 150 to 300 ms (~200–425) and is the thickest near the LR. Toward the Gakkel Ridge, subunit 1c shows a more variable distribution throughout the central basin (Figures 3a–3c).

Near the LR, subunit 1c is about 300 ms (~425 m) thick adjacent to the ridge flank and thins to about 150 ms (~190 m) toward the WAB, apparently influenced by a broad intrabasin topographic relief defined by the top of subunit 1b (dark blue horizon in Figure 3a). Likewise, seismic lines A91-098 and A91-100 (Figure 2) show distinct thinning of subunit 1c (to $<$40 ms) over an intrabasin high. However, the regional coherency of these basinal structures and resulting strata patterns cannot be established with the current data.

In the central WAB, subunit 1c shows onlap and thinning toward the basement highs (Figure 3). In some areas, evidence for slope instability and mass transport deposits are observed (Figure 9b). These areas are

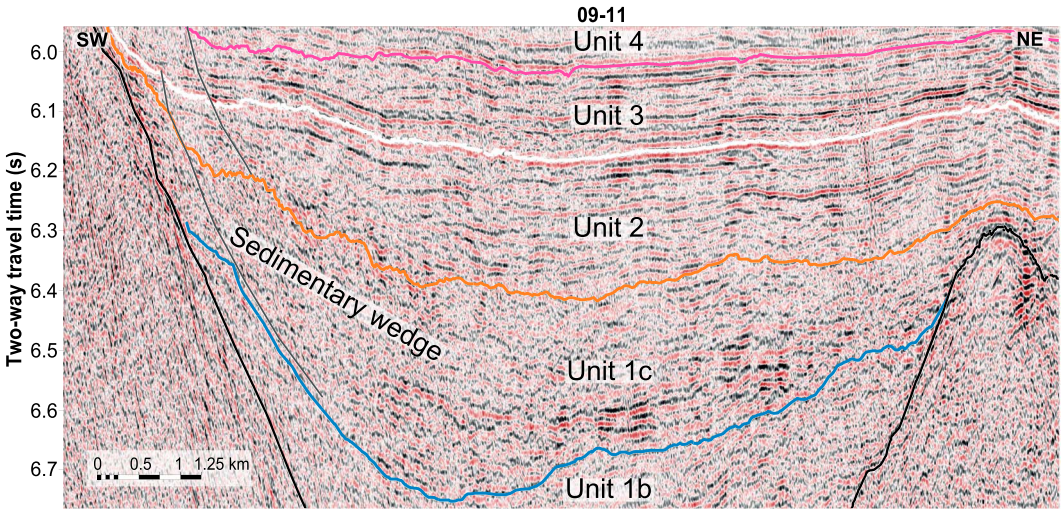

Figure 7. Detail from Figure 4 displaying a thick sedimentary wedge developed within subunit 1c and fault-bounded against the Lomonosov Ridge. The depositional body is characterized by an irregular surface with discontinuous seismic reflections that appear to offlap and downlap top subunit 1b (dark blue horizon). Key seismic horizons interpreted: oceanic basement = black; top subunit 1b = dark blue (C18o–C15y, 37.5 ± 2.5 Ma); top subunit 1c = orange (C18y–C12o, 27.5 ± 2.5 Ma); top subunit 2 = white ($<$C8y, $<$ 25–20 Ma); top unit 3 = magenta. y = young; o = old.

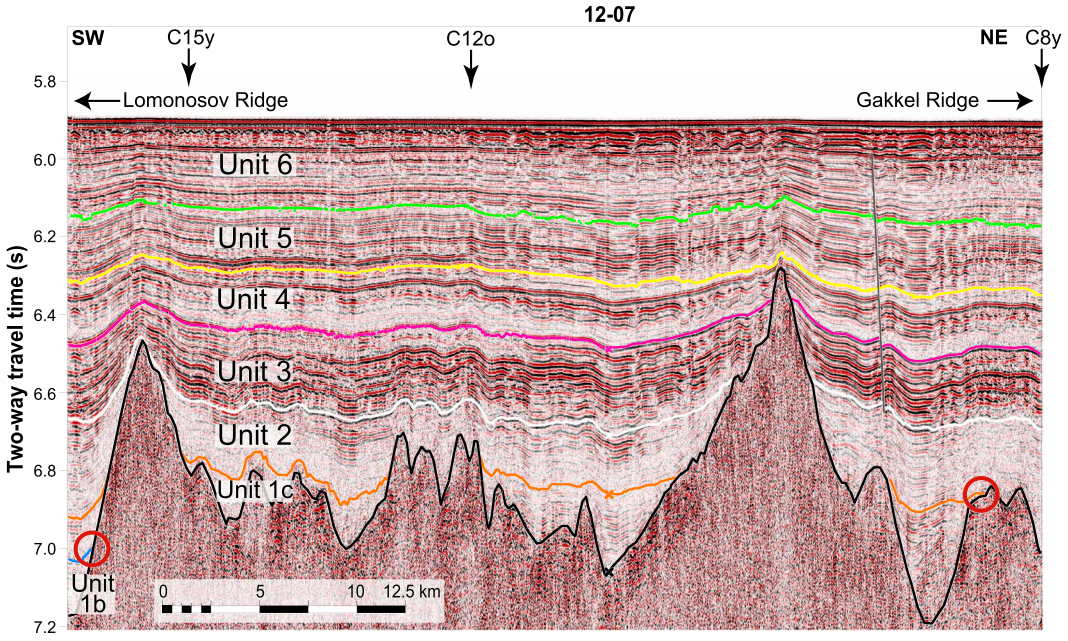

Figure 8. Seismic profile GEUS-LOMROG2012-07 crossing the western Amundsen Basin between Chrons C18o and C8y (see Figures 1 and 2 for line position). The large thickness observed in unit 2 at C8y suggests that the true chronostratigraphic pinchout for unit 2 lies beyond magnetic isochron C8y. Key seismic horizons interpreted: oceanic basement = black; top subunit 1b = dark blue (C18o–C15y, 37.5 ± 2.5 Ma); top subunit 1c = orange (C18y–C12o, 27.5 ± 2.5 Ma); top subunit 2 = white (<C8y, < 25–20 Ma); top unit 3 = magenta; top unit 4 = yellow; top unit 5 = green; top unit 6 = seabed. (red circles) Positions where the horizons onlap the oceanic basement (see Figure 2). y = young; o = old.

commonly related to deep-seated faults that bound the basement highs, suggesting active tectonism during deposition.

In the lower part of subunit 1c, a sedimentary wedge characterized by a steep, lenticular reflection pattern extends out from the LR (Figure 7). The wedge is about 3.5 km wide and has an approximate dip of 10°. The maximum thickness of the wedge is about 325 ms (~450 m) and pinches out toward the LR with strata downlapping toward the base horizon of unit 2 (Figure 7). Internal reflections of the wedge are weak and discontinuous to semichaotic. Similar wedge-like features are observed in other areas along the ridge flank (Figure 4) including Alfred Wegener Institute (AWI) line A91-097 (Jokat et al., 1995a).

4.1.2. Unit 2

Unit 2 ranges from about 120 to 270 ms (~140–310 m) thickness (Figures 3, 4, and 9) and is typically more transparent than unit 1, although it is occasionally marked by weak reflections showing a continuous to semicontinuous distribution (Figures 3, 9b, and S5). Toward the Gakkel Ridge, unit 2 shows a gradual thickening. In addition, local thickness decreases, and episodic truncation is observed over the topographic highs in the central basin (Figures 3a–3c). The draping monotonic sedimentary cover of this unit observed throughout the basin implies formation in a predominantly hemipelagic setting far from point sources of sedimentary input.

Near the LR, unit 2 has a relatively uniform thickness of about 225 ms (~275 m) along seismic profile LOMROG2009-11 (Figures 3a, 4, and 7); however, a distinct thinning of the unit (to <40 ms) similar to subunit 1c is observed over an intrabasin high along seismic lines A91-098 and A91-100 (Figure 2). Unit 2 therefore also seems to be affected by a broad-intrabasin topographic relief in some areas along the LR.

4.1.3. Unit 3

This unit is characterized by parallel, coherent reflections that show extensive lateral continuity (Figures 3a and S5). As a consequence, top unit 3 forms a distinct horizon that can be traced with a high degree of confidence throughout the WAB. Unit 3 has a relatively uniform thickness of 225 ms (~240 m) with a maximum of 260 ms (~270 m) in the central parts of the basin. Along seismic profile 09-11, unit 3 thins toward the ridge flank to about 80 ms (~100 m) and shows depositional pinch-out toward the underlying unit 2 (Figure 5). The

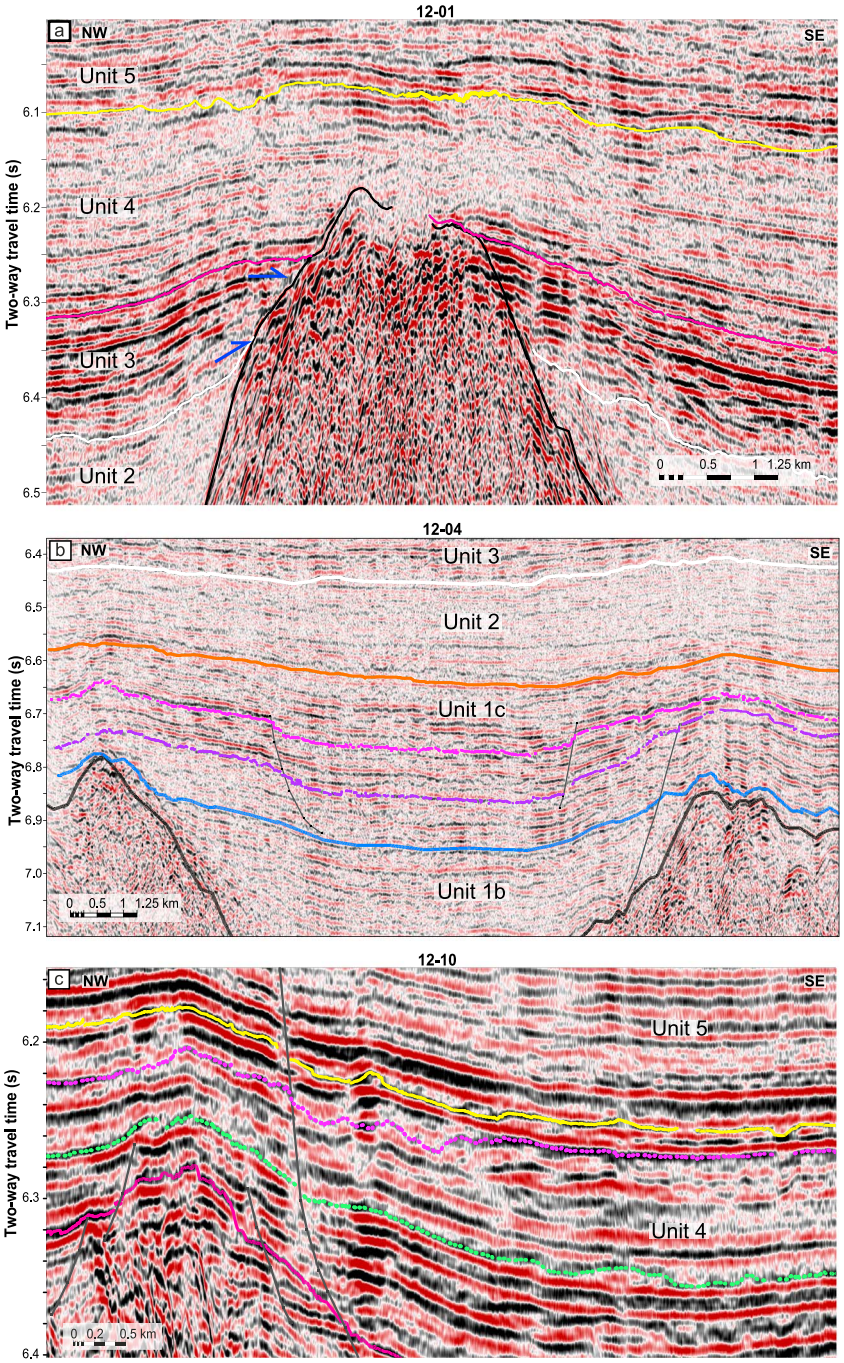

Figure 9. (a–c) Detailed images from Figures 3c and S5 showing structural influence on strata development and sedimentation patterns. (a) Strata dip changes in unit 3 along a basement structure (indicated by blue arrows). An upward decrease in dip of onlapping strata from 30° to 0°is observed. (b) Example of mass movements within subunit 2a related to slope instability and structural faulting along the flanks of a subbasin (internal horizons shown in red and purple colors). (c) Asymmetric mounded features seen within unit 4 (purple and light green hatchured markers) inferred as contourite drift deposits formed along a fault-bounded topographic high. Key seismic horizons interpreted: oceanic basement = black; top subunit 1b = dark blue (C18o–C15y, 37.5 ± 2.5 Ma); top subunit 1c = orange (C18y–C12o, 27.5 ± 2.5 Ma); top subunit 2 = white (<C8y, < 25–20 Ma); top unit 3 = magenta; top unit 4 = yellow. y = young; o = old.

strong, continuous reflection pattern seen in unit 3 combined with depocenter development in the central basin points to a predominantly hemipelagic depositional environment with limited input from marginal sources.

Thinning and occasionally truncation of unit 3 is seen over the protruding basement structures in the central WAB (Figures 3c and S5). In some locations, the thinning is associated with an upward decrease in dip of onlapping strata (Figure 9a). This suggests that deposition was influenced by local structural development of the central basement highs that could provide a sediment source from submarine weathering of oceanic crust.

4.1.4. Unit 4

Unit 4 varies in thickness from 125 to 190 ms (~120–180 m). In contrast to the underlying unit 3, this unit thickens from the central basin toward the LR (Figure 3a). Local thickness increases are seen to be associated with subbasin structures toward the Gakkel Ridge (Figure 3c). The unit consists of weak to poorly defined reflections, although some strong and laterally continuous reflections are also observed in some basinward locations (Figures 3a–3c and S5). In the central WAB, reflections are semiparallel but interspersed with hummocky geometries and occasionally gentle convex geometries that tend to form around basement highs due to differential compaction (Figures 3a–3c and S5).

LOMROG lines 09-11 and 09-10 show weakly developed mounded buildups juxtaposed on distinct topographic lows against the LR flank (Figures 4, 5, and S6). The widths and depths of the troughs, respectively, range from 1 to 1.5 km and 50 to 80 ms (~50–80 m). The asymmetric mounded geometries are characterized by internal discontinuous reflections formed above an erosive base at the top of unit 3. LOMROG line 2012-10 also displays a similar mounded expression of unit 4 perched against a topographic high (Figure 9c). Although the internal reflection patterns often appear dimmed or vaguely defined, aggradational geometries can be recognized (Figure 9c).

4.1.5. Unit 5

Unit 5 shows a consistent thickening from north to south, that is, toward the Gakkel Ridge, with basinal depocenters increasing from about 160 to 320 ms (~150 to 300 m thick; Figures 3a–3c). Unit 5 thins along the transect going from west to east (Figure S5). The LR profiles indicate the development of a more localized depocenter (>250 m thick) indicated by positive relief along the northern basin margin (Figures 3a and S6).

The seismic facies of unit 5 are characterized by coherent, parallel to semiparallel reflections across the basin (Figures 3a–3c and S5), although more uneven and discontinuous seismic facies are seen within the depocenter in vicinity of the LR (Figures 5, 6, and S6). Some of the seismic sections reveal an internal organization of unit 5 into several subunits that onlap the top unit 4 horizon in a direction toward the LR (Figures 3a and 3c). Internal reflections appear phase reversed (i.e., negative impedance contrast), which may suggest that the continuous reflectivity is caused by clayey intervals interspersed by more silty-sandy deposits. Below the LR flank, the seismic facies becomes less discontinuous with mounded geometries interspersed laterally with concave reflection patterns commonly showing erosive signatures (Figures 5 and 6). This reflection pattern is interpreted as incised channel segments that are up to 50 ms deep (~50 m) and 1 km wide, bounded by levee deposits. In the key profile, Figures 3a and 4, the channelized deposits are seen to accumulate over the inclined, unconformable top unit 4 horizon, which dips ~2° into the basin. The channel deposits infill the buried trough along the ridge flank (see also Figure S6).

4.1.6. Unit 6

The uppermost unit drapes the WAB and has a thickness that ranges from 125 to 250 ms (~100–200 m). The regional thickness variations and unit geometry indicates two depositional trends: (1) a small gradual increase in accumulation toward the basin sector bordering the Gakkel Ridge and (2) discrete, mounded sedimentary buildups associated with a recent channel system (Figures 3a–3c and S5). This channel accumulation is also imaged on the AWI lines east of the LOMROG transect in Figure 3a, suggesting that it extends at least up to 70 km from the flank of the LR.

The basinward accumulation of unit 6 is characterized by sets of strong, continuous reflections displaying a positive impedance (Figures 3a–3c and S5). They demarcate individual depositional units that internally show arcuate and contorted to chaotic reflection patterns. These depositional units tend to thicken into the low-relief subbasins and are defined by the top of unit 5. In some places, they are seen to evolve from erosional scarps and faults above deep structures. Based on the seismic expression, they are interpreted as mass-flow deposits, that is, debrites (Gong et al., 2014). Accordingly, the small-scale arcuate- clinoformal patterns may be overriding thrusted layers generated by slow-moving mass-transport processes, although it should be noted that these features approach the limit of seismic resolution (Figure 3c).

The accumulation zone of unit 6 along the LR is associated with a modern channel system, referred to as NP-28, that extends from the Lincoln Shelf margin into the Amundsen Basin (Kristoffersen et al., 2004; Svindland & Vorren, 2002). The channel itself, about 5 km wide and 80 ms (~60 m) deep, is marked by erosional surfaces separated by gentle scarps that back-step at three distinct levels toward the LR flank. The deepest channel segment is flanked by a scarp approximately 70 ms (~50 m) tall and dipping about 10° (Figure 5). The scarp truncates strata that form part of a prominent levee buildup on the basinward side. Offset reflections and discontinuities suggest the development of small growth faults within the levee deposits (Figure 5). The levee construction eventually merges with the abyssal plain >20 km away from the channel. Discontinuous, truncated reflection patterns displaying internal onlap and lenticular to concave features are seen below the modern channel (Figures 5 and S6). The channelized seismic facies suggests that high-energy current flows shape the modern seafloor and have been active throughout the deposition of the unit. The basal horizon (top unit 5) forms an erosional surface that demarcates a buried channel about 1.5 km wide and 50 ms (~40 m) deep, filled by small clinoforms (Figure 5). The position of the buried channel relative to the modern counterpart suggests that the main channel pathway has shifted 3.5 km in a basinward direction during deposition of the unit. A channel feature is also observed in the southern part of the WAB bounded by the outer Gakkel Ridge structure and a thick incised strata package, probably composed of units 5 and 6 (AWI-91-104; Figure 3c). Aside from its location and deeper bathymetry on the opposite side of the basin, this feature differs from the NP-28 system by its dimension (~150 vs. 60 m deep) and symmetric left-side levee formation. Hence, its mode of origin is most likely different from the NP-28 channel.

4.2. Chronology and Sedimentation Rates

The WAB contains a more than 2-km-thick, relatively conformable, and continuous seismic stratigraphic succession (Figures 3 and S5) forming a complete sedimentary record since the onset of deposition in the early Cenozoic. Because no deep borehole data are available, it is necessary to infer ages from the stratigraphic pinch-outs on oceanic basement. Stratigraphic ages can be estimated based on magnetic spreading anomalies of the underlying oceanic crust, providing a maximum possible age for a horizon as noted earlier (Figure 2). This primarily applies to the older units where the basement onlap relationships are clearly imaged on the limited seismic data. Here the magnetic anomaly interpretation of Brozena et al. (2003) is used, and ages are assigned based on the geomagnetic timescale of Ogg (2012). Jokat et al. (1995a) derived ages based on the magnetic anomaly interpretation by Vogt et al. (1979) using ages from Cande and Kent (1992), while Chernykh and Krylov (2011) provided their own anomaly interpretation calibrated to Cande and Kent (1995). We report horizon ages and sedimentations rates based on new data alongside the previously published results and their respective geomagnetic polarity timescales for better comparison (Figure 10).

Dating of the units using magnetic anomalies has a number of limitations. First, there is a large uncertainty due to the ultraslow spreading. Closely spaced anomalies are difficult to distinguish from shipboard and aeromagnetic surveys because the sensor is too far away from the anomalies (Russell, 1999). Second, the sparse seismic data coverage in the region spanning Chrons C25N–C23N (~57–53 Ma) introduces significant correlational gaps, leading to uncertainty of the age of the deepest units (in particular unit 1). Finally, rough basement topography can complicate the onlap relationships so that a horizon pinches out locally on older crust. For horizons dated this way, several seismic lines were checked when possible, and the pinch-outs were remarkably consistent relative to the magnetic anomaly pattern, giving some confidence that the approach provides reasonable age estimates. Thus, despite the drawbacks of dating seismic horizons this way, it remains the only option for the deeper units and provides some information for estimating sedimentation rates.

The range of sedimentation rates presented in Figure 10 includes the thickness variation between individual subbasins and variation in seismic velocities for each unit. Parameters for calculating sedimentation rates are shown in Table 2, and the locations of sonobuoys used for the velocity estimates are shown in Figure 2. To be as representative as possible, the sedimentation rates were calculated by combining the velocities and two-way travel time thickness observed along the different profiles (Figures 3a–3c and S5). If the measured two-way travel time thickness of a unit was located along a profile containing sonobuoy data, the 1-D velocity model was used to calculate the sedimentation rates. Otherwise, the sonobuoy closest to the measurement was used. If the measured two-way travel time thickness was located at a similar distance between two sonobuoys (e.g., LOMROG2007-01; see Figure 2), the sediment rates were calculated by averaging the

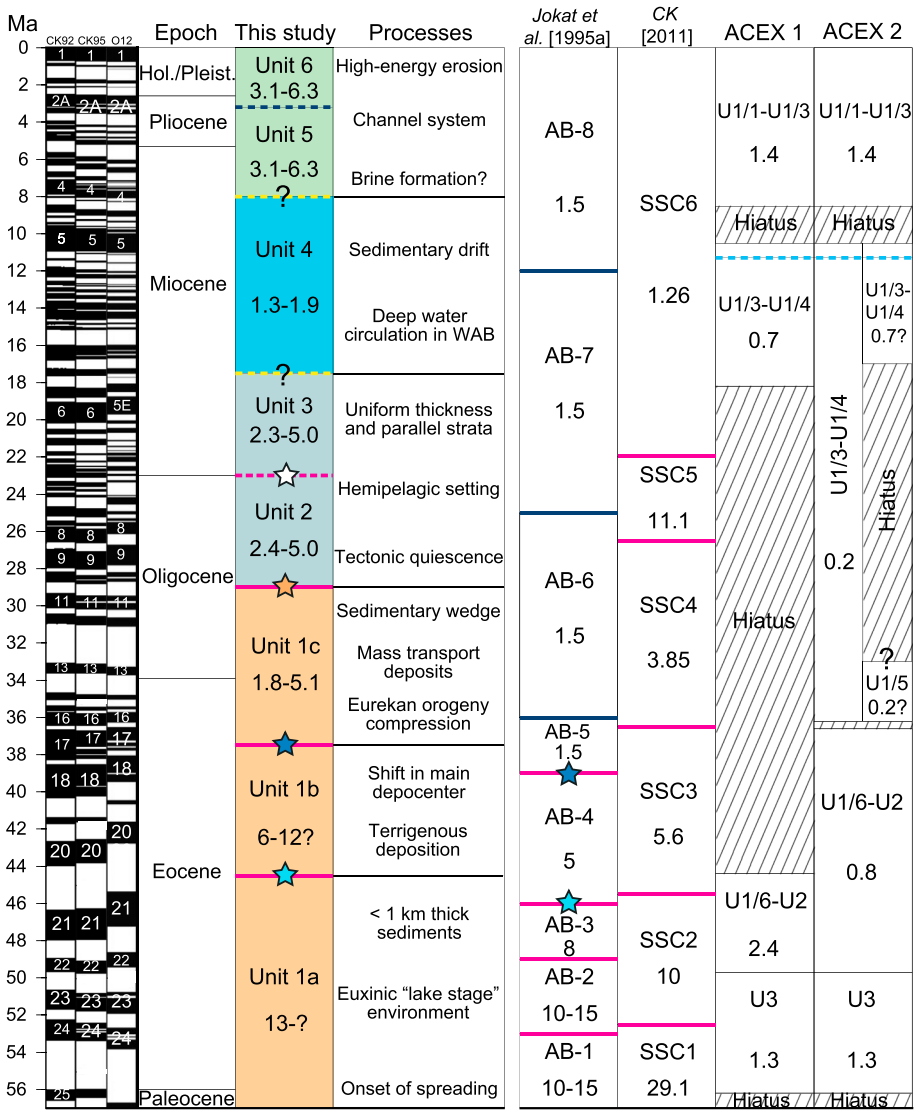

Figure 10. Seismic-stratigraphic units and horizon ages defined in the western Amundsen Basin compared to previous basin studies and the ACEX borehole stratigraphy. The numbers shown are the inferred sedimentation rates (cm/ka). Color coding indicates the four interpreted depositional environments discussed in the text. (magenta horizons and colored stars) Aeromagnetic dated boundaries (see also Figure 2). (yellow horizons) Boundaries inferred from oceanographic considerations. (dark blue horizons) Boundaries inferred from estimated sedimentation rates. (light blue horizons) Cosmogenic dated boundaries (Frank et al., 2008; recalibrated according to Chmeleff et al., 2010.). Geomagnetic polarity timescales based on Cande and Kent (1992; left), Cande and Kent (1995; middle), and Ogg (2012; right). (black) Normal polarity chrons. (white) Reversed polarity chrons. CK92 = Cande and Kent (1992); CK95 = Cande and Kent (1995); O12 = Ogg (2012); CK [2011] = Chernykh and Krylov (2011). ACEX = Arctic Coring Expedition.

velocities of the two sonobuoys closest to the profile. The velocity modeling and sonobuoy data are presented in Figures S1–S4. There are two main sources of error in the sedimentation rate estimates. One is uncertainty in the age estimates, and the second is with time-depth conversion. In the absence of direct sampling and age dating, the former is difficult to quantify. We include in the Table 2 and Figure 10 ranges that are considered reasonable, but it should be noted that these are not rigorous error bars.

For comparison to previous work, the correlative seismic units dated by Jokat et al. (1995a) are shown in Figure 10. Subunit 1a corresponds to seismic units AB-1 through AB-3 identified by Jokat et al. (1995a), while subunit 1b roughly corresponds to AB-4. For the remaining units, the ages between this study and the corresponding units differ due to the assumption made by Jokat et al. (1995a) of a constant sediment rate of about

Table 2
Chronology, Thickness, and Velocity Ranges Used for Calculating Sediment Rates

AB unit	Age of top horizon	Thickness (TWT)	Velocity(km/s)
Unit 6	—	100–200 m (125–250 ms)	1.54–1.6
Unit 5	4–2 Ma[a]	150–300 m (160–320 ms)	1.9–2.0
Unit 4	10.6–8 Ma	120–182 m (125–190 ms)	1.9–2.0
Unit 3	20–15 Ma	130–270 m (125–260 ms)	2.0–2.4
Unit 2	Younger than C8y (< 25–20 Ma)	140–310 m (120–270 ms)	2.1–2.4
Unit 1c	C18y–12o (27.5 ± 2.5 Ma)	190–430 m (150–300 ms)	2.5–2.8
Unit 1b	C18o–15y (37.5 ± 2.5 Ma)	470–910 m (375–700 ms)	2.6–2.9
Unit 1a	C21y–20o (44.5 ± 1.5 Ma)	1,500 m (925 ms)	3.1–3.2

Note. Only basinal thicknesses were used for calculating sediment rates, while sections influenced by tectonic factors (e.g., thin sediments above basement ridges) were omitted. Locations of key sonobuoys used for the velocity estimates are shown in Figure 2. The velocity modeling and sonobuoy data are presented in supporting information S1. Ages are calibrated according to the timescale of Ogg (2012) except for unit 6. TWT = two-way travel time.
[a]Based on estimated sedimentation rates.

1.5 cm/ka from the late Eocene onward for dating their remaining horizons (Figure 10). Based on the revised chronology, subunit 1c and unit 2 are largely equivalent to AB-5 and AB-6. Finally, the uppermost succession, represented by units 3–6, corresponds to AB-6 through AB-8 defined by Jokat et al. (1995a). Due to the sparse LOMROG data within the older part of the basin (Chron C21y onward), a subdivison of the oldest unit, 1a, into the three smaller units as defined by Jokat et al. (1995a) was not possible. However, two additional sedimentary units are identified, units 2 and 4, within AB-6 and AB-7, respectively. In addition, a more detailed description of unit geometries and seismic facies of the basin succession is presented, notably along the LR flank (Figures 3 and 4).

The ages of the horizons top units 1a–1c were assigned based on where the horizons onlap the oceanic basement (Figure 2). The approximate ages are 45, 38, and 29 Ma, respectively. These ages indicate that the early basin evolution corresponds to relatively high sedimentation rates, >10 cm/ka, peaking during the early Eocene (Figure 10). The ages for the horizons top units 1a and 1b are the most robust in the data based on the multiple locations where onlap is observed (Figure 2). These units correspond to the seismic units AB-1 through AB-4 identified by Jokat et al. (1995a), which were also dated by the same sections of onlap but using an alternate magnetic anomaly interpretation as discussed above.

This study differs in the dating method used by Jokat et al. (1995a) for subunit 1c and unit 2 (AB-5 and AB-6). In the model by Jokat et al. (1995a), AB-5 was calculated by assuming an average sediment rate of about 1.5 cm/ka and a 40 m thickness for the entire unit, yielding a span of ~3 Ma and an age of ~36 Ma for the top boundary of AB-5 (Figure 10). In contrast, this study incorporates the subsequent AWI data presented by Jokat and Micksch (2004). Whereas the original profiles by Jokat et al. (1995a) show gaps and/or high basement topography when crossing Chron C8y (e.g., A91-102 and A91-104 located in Figure 2), Jokat and Micksch (2004) show a continuous profile that appears typical for the basin (Figure S5). Thus, the age for unit 1c, corresponding to the lowermost interval of AB-5, was assigned based on the youngest two onlaps observed in the AWI and LOMROG data between Chrons C12o and C8y (Figure 8 and Figure S7).

The age of horizon top unit 2 was inferred from seismic profiles 12-07 and AWI2001-0300. In the AWI profile, a clear onlap for unit 2 is observed (Figures 2 and S7) at about Chron C8y (~25 Ma). This onlap coincides with regional basement shallowing toward the Gakkel Ridge. In the nearby LOMROG profile, unit 2 is observed at the same time interval with no clear onlap and no significant basement shallowing (Figure 8). Since unit 2 shows no significant thinning here and seems to continue beyond Chron C8y along 12-07, it is possible that this horizon is likely younger than 25 Ma, probably ~25–20 Ma. However, more data are required to validate and/or constrain the age for the top of unit 2.

The magnetic anomalies do not provide age constraints beyond Chron C8y (~25 Ma). Ages for units 3–6 are estimated based on comparison to previous work and correlations with changes in facies patterns that can be related to known tectonic and oceanographic events in the Arctic Ocean. The top of unit 3 is assigned an age of 20–15 Ma based on the inferred onset of a ventilated regime in the Arctic Ocean according to age model 1 (Figure 10). Thus, we correlate the oxygenated late Miocene interval in the ACEX record (starting at 193-m

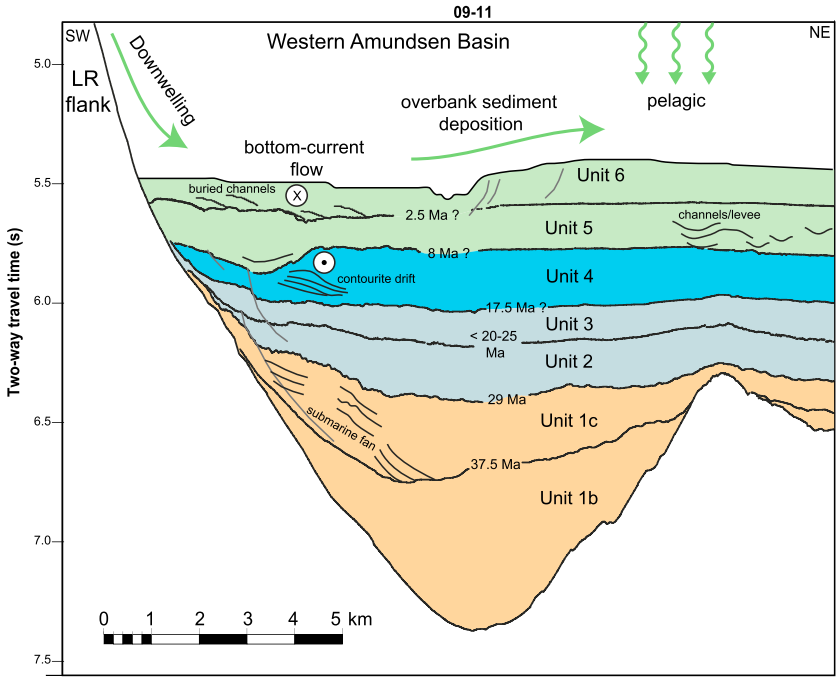

Figure 11. Line drawing of profile LOMROG2009-11 (Figures 4–7) with inferred depositional environments and horizon ages. Main sedimentary pathways are indicated by green arrows. Ages for units are derived from ties to the magnetic anomaly interpretation of Brozena et al. (2003). Color coding same as Figure 10. LR = Lomonosov Ridge.

core depth) to a phase of sediment drift accumulation along the LR indicated within unit 4. The top of unit 4 is assigned an age of 10.6–8 Ma based on correlation to a ^{10}Be dated hiatus at 135.5–140.4 m in the ACEX core (Frank et al., 2008; recalibrated according to Chmeleff et al., 2010) and the onset of ferromanganese crust growth on the LR flank (Knudsen et al., 2017). This latter observation is consistent with the onset of a higher energy environment inferred above unit 4 and that is necessary for the crust to grow and be preserved (Föllmi, 2016). Unit 4 thus was deposited during a relatively long interval of slow sedimentation (rates estimated between 1.3 and 1.9 cm/ka). The lower end of this range is comparable with that found in previous studies for the same interval corresponding to seismic units AB-6 through AB-8 (Jokat et al., 1995a).

An age of 8 Ma for the top of unit 4 yields gross sedimentation rates between 3.1 and 6.3 cm/ka for the youngest units, 5 and 6. This is within the lower range of the shallow core results obtained by Svindland and Vorren (2002; 5.9–24.7/ka over the last 17 ka) and Backman et al. (2004; 1–25/ka). The rates imply that the base of unit 6 is approximately 2–4 Ma, that is, late Pliocene–early Pleistocene.

5. Sedimentary and Paleoceanographic Evolution of the Amundsen Basin

Analyses of the LOMROG seismic data and the tie of key horizons to the magnetic stratigraphy of the Arctic Ocean (4.2) provide significant new input to the evolution of the WAB (Figure 11). The Cenozoic development is discussed based on seismic geometries and facies pertaining to the updated stratigraphic scheme of the present study. The paleoceanographic history inferred from our results is discussed in relationship to previous studies that notably builds on the sedimentary records derived from the ACEX samples. As noted earlier, recently published age models have called into question the nature of the late Eocene-mid-Miocene hiatus based on earlier ACEX results. In this discussion, the original ACEX age model (Backman et al., 2008) is used. The implications of the alternative age model (Poirier & Hillaire-Marcel, 2009, 2011) are considered in a separate subsection.

5.1. Eocene-Early Miocene Evolution (Units 1–3)

Deposition of subunit 1a began from the onset of spreading in WAB in the late Paleocene at ~57 Ma until the mid-Eocene at ~45 Ma. LOMROG lines 07-01, 09-12, and 12-11 (Figure 2) indicate thicknesses greater than 1 km and thus high sedimentation rates. This likely reflects enhanced supply of terrestrial material,

possibly derived from weathering and erosion from the LR, although sediments may have also originated from regional highs that are now at conjugate positions, for example, the Barents Shelf and Yermak Plateau margins. The high sedimentation rates may also be linked to increased pelagic deposition associated with high biological productivity (Stein et al., 2006) that characterizes the early–mid-Eocene greenhouse climate conditions (Zachos et al., 2008). Moreover, an intensified hydrological cycle (Carmichael et al., 2016; Pagani et al., 2006) resulting in episodic fresh water accumulation (Brinkhuis et al., 2006) apparently enabled high biological productivity as evidenced by the large quantities of the freshwater fern Azolla in the central Arctic (Brinkhuis et al., 2006; Speelman et al., 2009; van der Burgh et al., 2013) and in adjacent regions (e.g., Collinson et al., 2010).

The upper range of the sedimentation rates for subunit 1a is poorly constrained due to sparsity of data within the older part of the basin (Chron C21y onward). Although precise paleowater depth estimates for the LR are challenging due to the absence of micropaleontological markers in the ACEX record, benthic-agglutinated foram assemblages dated around the Paleocene-Eocene thermal maximum (~55 Ma) suggest that the LR was close to sea level at that time (O'Regan et al., 2008).

Deposition of subunit 1b, approximately mid-Eocene to late Eocene, is marked by a decrease in sedimentation rates compared to subunit 1a (Figure 10). The lower range of the rates estimated, 6 cm/ka, is roughly in accordance with previous studies, while the higher range, 12 cm/ka, is based on a thick development of the unit seen in the central WAB (Figure 3b). The observations from the LOMROG seismic data imply that the position of the main depocenter during the late–mid-Eocene shifted toward the center of the basin near 07-01 (Figure 2).

The subunit 1c wedge infills the Amundsen Basin asymmetrically from NW to SE toward the Gakkel Ridge (Figures 3, 4, and 7). This subunit was deposited between 37 and 29 Ma corresponding to the late Eocene to mid-Oligocene epochs. Low-angle progradational features are observed, suggesting lateral transport of sediments away from the LR toward the central basin. The evidence for slope instability and mass transport (Figure 9b) that appear to correlate with sediment transport over the basement highs (Figure 9) suggests that tectonic instability influenced the late Eocene-mid-Oligocene basin development phase. Steeply dipping reflections, bounding wedge-shaped bodies, seen within subunit 1c are interpreted as submarine fan deposits extending from the ridge flank (Figure 7). Similar features, but more vaguely defined, are seen on other profiles along the LR flank (e.g., 09-07 located in Figure 2) and A91-097 (Jokat et al., 1995a). This suggests that sediments were actively eroded from the LR where it merges into the Lincoln Shelf margin.

Jokat et al. (1995a) suggest that the mid-Eocene (46 Ma) marks the onset of LR subsidence to greater depths, shifting the depositional style in the Amundsen Basin from slope-rise to pelagic sedimentation. This may have been accompanied by deposition of biosiliceous ooze deposits with an admixture of terrigenous material along the basin margins. An increase in ice-rafted debris from 47 Ma has been related to an early cooling phase and the initiation of sea ice and glacial ice in the Arctic Ocean (St. John, 2008; Stickley et al., 2009).

Sedimentary subunits 1b and 1c (mid-Eocene to mid-Oligocene) correspond to the lower half of the 44–18 Ma depositional hiatus inferred in the original study of the ACEX cores (Backman et al., 2008; Figure 10). This time gap overlaps the main phase of Eurekan compression in North Greenland, Ellesmere Island, and Svalbard from 55 to 33 Ma (e.g., Gion et al., 2016; Oakey & Chalmers, 2012; Oakey & Stephenson, 2008; Piepjohn et al., 2016). Several recent studies suggest that the Eurekan orogeny affected large parts of the Arctic Ocean (Døssing, Hopper, et al., 2013; Døssing et al., 2014; O'Regan et al., 2008). In particular, gravity inversion shows that Eurekan compression may have affected the oceanic crust of the Amundsen Basin, the western LR, and below the Lincoln Shelf toward the Morris Jessup Rise, including crustal thickening and uplift of the LR plateau (Døssing et al., 2014). Ensuing erosion from uplifted areas may have been more significant on the shallower parts of the LR closer to the Greenland margin than at the deeper portions lying nearby the ACEX site. The present day depth of LR near Greenland is ~600 m, whereas the ACEX site is at 1,200 m. Although Eocene reconstructions of paleowater depths exist for the central LR (e.g., Mann et al., 2009; O'Regan et al., 2008), there is limited information for the portion of the LR closest to the Lincoln Shelf. Thus, shallow or even subaerial areas near the Lincoln Shelf could have also served as an additional source for erosion and deposition. In the context of the regional tectonic configuration, it is most likely that the sedimentary signatures, for example, sedimentary wedges, observed within subunit 1b and 1c are linked to compression along the LR associated with Greenland's northward motion into the Arctic Ocean.

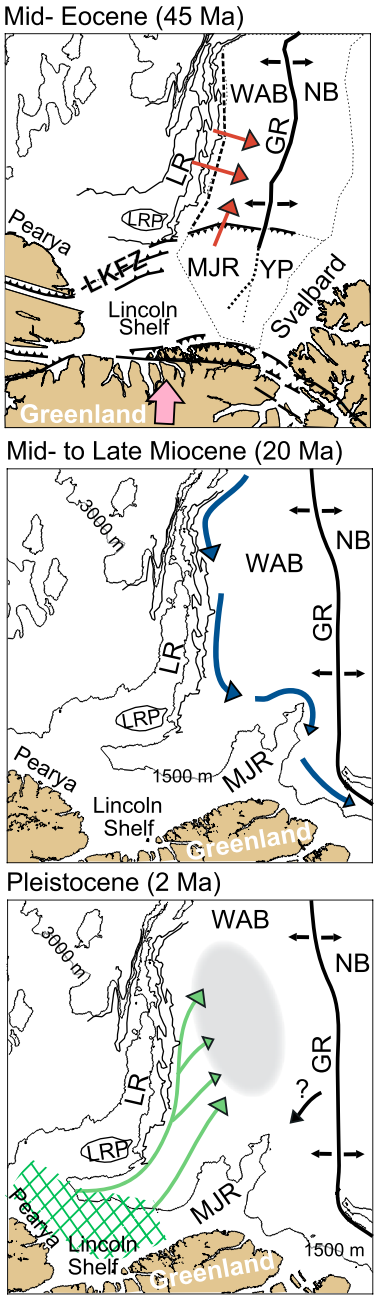

Figure 12. Conceptual scenarios illustrating the gross depositional evolution in the western Amundsen Basin since the mid-Eocene. The panels show kinematic evolution of key features using present day contours. (top) Middle Eocene (about 45 Ma) modified from Døssing, Hopper, et al. (2013). The main faults of the Eurekan compression and main crustal discontinuities/transforms (dashed/dotted lines) are shown. Pink arrow indicates the direction of Greenland motion. Black arrows indicate seafloor spreading; red/brown arrows indicate sediment transport from possible source areas. (middle) Mid- to late Miocene (about 20 Ma). Blue arrows indicate potential pathway of geostrophic currents along the base of slope. (bottom) Plio-Pleistocene scenario. Green arrows indicate channel pathways linked to brine formation and dense shelf water cascades. The Plio-Pleistocene depocenter (units 5 and 6) in the central basin is marked in gray. GR = Gakkel Ridge; LR = Lomonosov Ridge; LRP = LR Plateau; MJR = Morris Jessup Rise; NB = Nansen Basin; YP = Yermak Plateau; WAB = western Amundsen Basin.

The magnetically defined chronology of units 1b and 1c timing would fit into a model, whereby the LR was tectonically active and experienced postbreakup uplift during the late Eocene (Figure 12; Døssing et al., 2014; O'Regan et al., 2008; Minakov & Podladchikov, 2012).

In comparison with the high accumulation rates that characterize the Eocene, units 2 and 3 appear as condensed intervals with inferred sedimentation rates between 2.3 and 5.0 cm/ka (Figure 10). Based on the character of passive infill (e.g., parallel strata with basal onlap toward the LR), it is suggested that these units were deposited primarily by pelagic sedimentation in a relatively low energy environment. Thus, their signature appears associated with a period of limited tectonism following the Eurekan compression. The onset of a reduced stress regime along the LR likely ended in the middle-late Oligocene after which the proto-Fram Strait oceanic gateway may have begun to form through in response to trans-extension and subsidence (Engen et al., 2008; Jakobsson et al., 2007).

5.2. Mid-Miocene-Late Miocene Evolution (Unit 4)

The thickening of unit 4 along the base of the LR is consistent with an origin related to oceanographic bottom currents (Figure 3a). Although downslope processes, for example, local submarine fans, may also be considered for this margin-bound depocenter, the lack of sedimentary input sources is conspicuous. Moreover, the buried, asymmetric mound-moat geometries along the ridge flank (Figures 3a, 4, and S6) and the low-relief mounded accumulations over some of the structural highs (Figure 9c) are reminiscent of contourite drifts that commonly drape the lower slope of continental margins (Rebesco et al., 2014). The buildup of contourites reflects enhanced deposition of fine-grained sediments along the fringe of bottom-current pathways that are generally controlled by large-scale meridional overturning circulation. Flow speeds that favor drift accumulation are commonly in the range of 5–15 cm/s, while erosional elements, for example, at the base or within juxtaposed moat-channels, imply velocities exceeding 25 cm/s (Hernández-Molina et al., 2008). Contourites are widespread within the high-latitude ocean basins, ranging in scale from small patch drifts (10–100 km^2) to giant elongated drifts (>100,000 km^2; Faugères & Stow, 2008; Rebesco et al., 2014). In the Arctic region of the North Atlantic, slope-controlled contourite drifts are documented along the Western Spitsbergen margin (Rebesco et al., 2013), the eastern Fram Strait (Howe et al., 2008), and the Yermak Plateau (Mattingsdal et al., 2014). By analogy with these areas of current-induced sedimentation, unit 4 was likely influenced by geostrophic bottom currents flowing along the LR and tracing minor topographical variations within the WAB. Theoretically, this paleo-current system would follow the modern counterclockwise circulation pattern of the Arctic (Rudels, 2012) and thus flow from the Laptev Shelf margin toward Greenland as shown in Figure 12.

The lack of any robust dating for the horizons bounding unit 4 adds uncertainty to the onset of geostrophic flow responsible for focused sedimentation along the LR. However, since the drift formation is associated with large-scale movement of bottom waters, thus implying a full-scale ventilation of the Arctic Ocean, unit 4 is likely linked with a deep water connection through Fram Strait gateway. Different timings have been proposed for when this deep-water connection between the North Atlantic and the Arctic Basin became established. Wolf-Welling et al. (1996) proposed

a late Miocene gateway based on sediment samples. This contrasts with tectonic reconstructions (Engen et al., 2008) and ACEX core data (Jakobsson et al., 2007) that suggest an early Miocene timing. More recent studies based on seismic interpretation studies along the Yermak Plateau that include ties with paleomagnetic and biostratigraphic age constraints from Ocean Drilling Program drill sites favor a mid-Miocene age (Geissler et al., 2011; Mattingsdal et al., 2014). The timing of a late Miocene onset of deep-water circulation in the Arctic Ocean is synchronous with the formation of the major North Atlantic drifts (Wold, 1994) and is also recognized as a major phase in sediment drift accumulation in Baffin Bay (Knutz et al., 2015). Comparing the broadly defined seismic stratigraphic chronology with records from the North Atlantic and Baffin Bay makes a mid-Miocene age (20–15 Ma) seem most likely for the onset of current-induced deposition along the LR (Figure 11).

The commencement of the sedimentary drift in unit 4 likely corresponds to a full ventilation of the Amundsen Basin associated with a deep Fram Strait opening. The section of reddish heterogenic mudstone above 193 mcd at the ACEX site may provide a suitable sedimentary analog to the contourite drifts observed in unit 4. A paleomagnetic age of 17–18 Ma at the base of this interval provides a minimum age but an older onset, for example, 20–25 Ma, of a fully ventilated oceanic regime cannot be ruled out (Geissler et al., 2011; Mattingsdal et al., 2014). Moreover, an alternate age model for the ACEX site has been suggested based on recent data (see section 5.3 below). The preferred stratigraphic model based on the new seismic data and all previous work indicates relatively low average sedimentation rates for unit 4 (Figure 10). This may suggest that the current-induced sedimentation was intermittent and/or that the unit bounding unconformities contain significant depositional gaps (Figure 5).

5.3. Implications of an Alternate Age Model (ACEX 2)

In the previous sections, the discussion of the seismic-stratigraphic interpretation was within the context of the original age model from the ACEX results. However, the Paleogene chronology of the Arctic Ocean, and in particular the tectonic history leading to the transition from a lake to a full marine setting, was contested by Poirier and Hillaire-Marcel (2009, 2011) based on Re-Os isotope analyses. Their alternate age model (ACEX 2) suggests that the transition from an isolated, euxinic lake-stage to a semiventilated ocean basin occurred in the lowermost Oligocene at about 36–37 Ma rather than in the early Miocene as proposed by Jakobsson et al. (2007). Following this oceanographic event and a small hiatus (~0.4 Ma), a 5.7-m interval of gray- and black-colored mudstone was deposited, informally known as the *Zebra unit* (ACEX unit 1/5). Poirier and Hillaire-Marcel (2009, 2001) interpreted this as an estuarine transitional phase when bottom water oxygen levels fluctuated over the LR. While the age of the base of unit 1/5 is constrained, the Os-isotope stratigraphy is inconclusive concerning the duration of the transitional interval. Therefore, uncertainty remains as to when the Arctic Ocean became fully ventilated. A simple linear interpolation between the Re-Os isochron age at the base of unit 1/5 and the oldest ^{10}Be age (of ~ 11.3 Ma (Frank et al., 2008; recalibrated according to Chmeleff et al., 2010) yields an apparent sedimentation rate of approximately 0.2 cm/ka. However, Poirier and Hillaire-Marcel (2011) note that in the absence of terrigenous input, such low sedimentations would require much lower ^{187}Os/^{188}O values due to the concurrent influence of global cosmic dust. Thus, higher sedimentation rates within the Zebra unit are likely and one or more condensed sections, or hiati, may exist above the onset of estuarine conditions at 36 Ma. In particular, the lithological contact between units 1/4 and 1/5 at ~193 mcd is consistent with an abrupt change from oxygen deficient to oxygen rich bottom water conditions (Moore and the Expedition 302 Scientists, 2006b).

The geodynamic model by O'Regan et al. (2008) and the notion of a delay in ridge subsidence due to compression were criticized by Chernykh and Krylov (2017). Based on a revised seismostratigraphic model for the central Amundsen Basin, the authors argue that the brief hiatus at 36–37 Ma and the low sedimentation rates within unit 1/5 were caused by a sea-level rise due to influx of Atlantic waters. However, the observation of the late Eocene-early Oligocene downlapping wedge extending from the ridge in unit 1c and the presence of a large depocenter in 1b suggests that a substantial terrigenous input in the Amundsen Basin remained prevalent until at least early Oligocene times. This late Eocene-early Oligocene timing would also broadly coincide with a phase of tectonic instability indicated by folding of sedimentary packages in the eastern Amundsen Basin (Gaina et al., 2015) and an observed seismic unconformity along the LR (Bruvoll et al., 2010). This high volume of terrigenous input would therefore likely match older multiproxy, geochemical, and sedimentological interpretations linking shallow waters in the central LR to higher depositional rates before the hiatus (März et al., 2011; O'Regan et al., 2008; Sangiorgi et al., 2008).

Poirier and Hillaire-Marcel (2011) argue that a possible marine invasion at 36 Ma reflects basin wide ventilation of the Arctic Ocean via a crustal stretching-created corridor within the proto-Fram Strait. Here it is questioned whether basin wide ventilation at this stage is consistent with plate-tectonic constraints on the opening of the Fram Strait. Following a prolonged phase of compression during the Eurekan and Svalbardian orogenies from 56 to 33 Ma (O'Regan et al., 2008), plate reconstructions show that the crust in northeast Greenland and west of Svalbard experienced trans-extension beginning in the Oligocene around 30 Ma. Major extension followed much later (Gion et al., 2016). This does not fit with opening a seaway connection already at 36 Ma. Seismic refraction data on Svalbard show that present day crust is 32–33 km thick (Ritzmann et al., 2004), and surface wave dispersion and receiver function analyses show that northern Greenland crust is 30–37 km thick (Dahl-Jensen et al., 2003; Gregersen et al., 1988). Assuming that the compressionally thickened crust in the proto-Fram Strait was on the order of 35 km thick and that 30 km thick is isostatically at sea level, exceptionally fast and geologically unreasonable strain rates would seem to be required to thin sufficiently to open a significantly wide and deep gateway before the Miocene.

Consequently, the estuarine regime with fluctuating oxygen levels conditions implied by the Zebra zone was most likely controlled by at most a shallow connection across the proto-Fram Strait (Engen et al., 2008). The regional crustal-tectonic constraints and the seismic-stratigraphic evidence indicating a high sediment supply to the WAB suggest that the estuarine transitional phase (Poirier & Hillaire-Marcel, 2011) was associated with vertical adjustments along the LR. This is consistent with the hypothesis of a compressional tectonic regime that delayed the submergence of the LR (O'Regan et al., 2008) although we cannot rule out that other factors, for example, oceanographic, may have played a role (Chernykh & Krylov, 2017).

It is possible that erosion of LR prior to submergence may be linked to the sharp contact between units 1/4 and 1/5 in the ACEX samples. The duration of a hiatus at this level is uncertain, but given a depositional rate of about 0.2 cm/ka of the Zebra zone (Poirier and Hillaire-Marcel, 2011), the hiatus extends from ~33 to 17 Ma (ACEX 2 in Figure 10). However, erosion linked to compression may have been more intense on the shallow ridge segment toward the Lincoln Sea compared to the deeper lying central portions in vicinity of the North Pole. Thus, the ACEX record may not accurately record the depositional changes that we infer for the WAB based on the present seismic data.

5.4. Late Miocene-Quaternary (Units 4–6)

Seismic reflection geometries showing present and buried channel features within units 5 and 6 provide evidence for confined and apparently erosive bottom currents trailing the northern margin of the WAB.

5.4.1. Channel-Levee Development Along the LR

Erosional features observed in unit 6 and the seafloor horizon below the LR flank include back stepping scarps and channel incision (Figure 6), suggesting a high energy environment associated with deposition of sand and winnowing/bypass of fine-grained sediments (Pickering et al., 1995). The transport of sediments in the fine sand fraction would require average current speeds $>$30 cm/s, that is, far greater than the geostrophic speeds normally associated with oceanographic boundary currents (McCave & Hall, 2006). The development of a prominent basinward levee suggests that the channel morphology was maintained by overbank deposition of muddy sediments carried by suspension currents periodically spilling over the channel pathway. This asymmetry of the channel profile is similar to other high-latitude sediment transfer systems of the northern hemisphere where downslope currents are deflected to the right into the basin due to the pronounced Coriolis effect (e.g., Klaucke et al., 1998; Menard, 1955). The high-amplitude discontinuous seismic facies of unit 6 continues into the basin, implying that the unit corresponds to a period of enhanced current influence on sedimentary deposition and distribution in the WAB. This interpretation is supported by fining-upward sandy facies interpreted as distal turbidite deposits observed in shallow cores (Fütterer, 1992; Svindland & Vorren, 2002).

It is uncertain when the high-energy depositional phase along the LR began, but it may be associated with a hiatus observed in the ACEX cores (Frank et al., 2008) and the onset of Fe-Mn crust formation on the ridge flank (Knudsen et al., 2017), suggesting an age of 10.6–8 Ma (Figure 10). The channelized sedimentary regime observed in units 5 and 6 is thus tentatively correlated to the U 1/1-U 1/3 interval of the ACEX record, which represents large scale-glaciation of the northern hemisphere (Zachos et al., 2001). The lower sedimentation rates of the ACEX sequence compared to the Amundsen Basin record reflects the hemipelagic environment of the ridge that is isolated from downslope sources. Based on typical sedimentation rates of high-latitude

channel systems influenced by turbidite overbank deposition, sedimentation rates on the thickest part of the levee (unit 6) may be as high as 25 cm/ka (Svindland & Vorren, 2002). However, average values integrated over longer time scales are likely to be an order of magnitude lower (Backman et al., 2004).

A crucial question relates to the flow mechanisms that generated the channelized seismic pattern and reflection truncation that mark the boundaries of units 5 and 6. The erosive character of the seabed suggests that the dominance of vigorous currents takes place at present, or at least, is a very recent phenomenon. Thus, it could be related to processes occurring during both glacial and interglacial periods. Dilute suspension currents operating on distal submarine fans are conventionally driven by high fine-clastic yields produced by fluvial-deltaic systems (Kneller & Buckee, 2000). The release of suspension-driven currents can be triggered by high fluvial discharges forming hyperpycnal plumes (Mulder & Syvitski, 1995; Parker, 1982). This latter process is particularly well-described for the Laurentide Fan in the Labarador Sea where sedimentary records show a high frequency of graded beds related to meltwater plumes (*plumites*; Piper et al., 2012). Radiocarbon dating of these deposits indicate that the discharges were primarily released during deglaciations or major collapse phases of the Laurentide Ice Sheet and related to Heinrich events (Rashid et al., 2003). However, observations from temperate glacial margin environments are not transferable to the Northern Greenland margin where meltwater production is severely limited by extremely low temperatures and precipitation (mean temperature ranges from -33 to 0 °C, and net annual precipitation is typically about 150–200 mm; Serreze & Barry, 2005). Considering the extreme climate condition of the North Greenland-Arctic margin, which is presently dominated by $>$2-m-thick multiyear sea ice (Lindsay & Schweiger, 2015), it is difficult to envisage a meltwater-driven mechanism as the primary factor for the recent development of channels and channel related deposits.

Based on seismic reflection data collected mainly from drifting ice stations, Kristoffersen et al. (2004) proposed the existence of a submarine fan in the Amundsen Basin. The authors suggest that this fan is associated with the NP-28 channel system and developed during the Pliocene-Pleistocene as a product of enhanced glacial sediment input in the sea passage between the Lincoln Shelf margin and the LR. The seabed morphology and spatial distribution of the NP-28 channel was further characterized by Boggild and Mosher (2016) using shallow seismic data. The depocenter geometry of the fan system extending from the Lincoln Shelf is contested by Døssing et al. (2014) based on excess sediment thickness mapping that indicate a separation between sediments confined along the LR near the North Pole and sediments further south in vicinity to the North Greenland margin. Thus, even though enhanced glacial sediment delivery to the shelf edge was likely important, other processes have to be considered given the basinal distribution of late Cenozoic depocenters with high accumulation rates and the low potential for glacial meltwater generation.

5.4.2. Brine Formation as a Mechanism for Enhanced Sedimentary Fluxes

As an alternative to meltwater-driven density currents operating on conventional high-latitude fans, the possibility that the channel development within units 5 and 6 is related to dense brines generated from annual sea-ice formation is considered (Rudels, 1995). Modern oceanographic studies suggest that brine formation is an important factor for Arctic deep-water formation, although evidence to constrain these processes and the vertical fluxes in the Arctic Ocean is sparse (Haley et al., 2008; Jones et al., 1995). Conversely, brine formation linked to cooling and sea-ice production in polynya regions is a well-documented on Antarctic margins where it contributes to the generation of Antarctic bottom water, for example, Weddell Sea (Gill, 1973; Smith et al., 2010), the Ross Sea (Assmann et al., 2003), the Adélie Coast (Kusahara et al., 2011; Marsland et al., 2004), and East Antarctica (Ohshima et al., 2013). Density stratification and water mass instability in these regions have also been linked to supercooling as the brines pass below thick permanent ice shelves at depths $>$100 m (Foldvik & Gammelsrød, 1988). As the cascades of dense, saline water masses enter the slope regime, energetic bottom currents are produced with speeds recorded of up to 50 cm/s (Ohshima et al., 2013). These currents are able to winnow and erode shelf and slope deposits (Presti et al., 2003) and thus may be an important factor in the formation of gullies and channels that are widely observed along the Antarctic margins (Gales et al., 2013).

In the Arctic Ocean, a model-based study by Backhaus et al. (1997) invokes sediment plumes triggered by brine release and polynia surface cooling as an important process driving vertical water mass exchange on the Eurasian Arctic margins. The shelf area north of Greenland is a potential source area for cascading brine plumes similar to the processes observed on the Antarctic margins. At the ACEX site, brine-driven water mass circulation has been inferred from radiogenic isotope studies of late Cenozoic material (Haley et al.,

2008). In that study, the Siberian shelf regions are inferred as the main source area of the brines, but since the ridge site is at a depth of intermediate water masses, the geochemical signatures cannot be compared to the deep-water setting of the WAB.

The LOMROG data suggest that the main accumulation area of the Pliocene-Pleistocene package was located in the central parts of the basin, while a secondary depocenter is associated with levee buildup along the NP-28 channel (Figures 3, 5, and S5). Bathymetric data suggest that the NP-28 channel branches off into the basin before reaching the North Pole (Boggild & Mosher, 2016). The branching, possibly related to levee breaching (avulsion) and Coriolis current deviation, points in the direction of the principal depocenter in the central basin. However, the present data coverage prevents firm conclusions on the regional distribution of transport pathways. It is possible that, rather than being supplied uniformly from the Nares Strait and Lincoln Shelf region, the sedimentary basin infill of units 5 and 6 originated from a broader area of North Greenland and Morris Jessup Rise, transported by dense sediment-laden plumes formed by surface cooling and brine-rejection (Figure 12). The channelized features seen within unit 5 could potentially form the distal component of fluvial systems active on the North Greenland margin during the Pliocene–early Pleistocene warm periods (Funder et al., 2001). However, for unit 6, associated with thick Arctic sea ice and the extreme cooling and major sea-level low-stands of the late Pleistocene, brine-related plumes are suggested as a more feasible mechanism for carrying sediments far into the basin. This process may also be important as a source for Arctic deep water, thus maintaining the baroclinic pressure gradient that drives southward export of water masses through the Fram Strait (Mauritzen, 1996; Rudels, 1995; Rudels et al., 2002).

6. Conclusions

Interpretation of new multichannel seismic reflection data is used to constrain the Cenozoic depositional history in the WAB and the adjacent LR. The study reveals a more detailed picture of the sedimentary packages than previously described (Chernykh & Krylov, 2011; Jokat et al., 1995a; Kristoffersen et al., 2004) and provides new insights into bottom current activity and sediment transport in an area that is largely unknown due to the challenges of acquiring data in the high Arctic.

Four main phases of basin development are identified (Figure 12):

- From the onset of seafloor spreading up to the mid-Oligocene, a small, isolated basin dominated by processes that were tectonically controlled is indicated. The high sedimentation rates in this period are linked to terrestrial material and increased pelagic deposition in a dominantly freshwater environment (Brinkhuis et al., 2006).

  Mass transport from structural highs filled a large depocenter with sedimentary wedges. These are linked to the Eurekan compression that resulted in uplift and possibly erosion of the Lomonsov Ridge adjacent to the Lincoln Sea. This interpretation is consistent with recent data showing that the ridge is thicker and shallower than the ridge at the ACEX drilling locations (Døssing et al., 2014). This has important implications for understanding the early subaerial exposure and subsidence history of the ridge compared to that inferred from the ACEX cores (e.g., O'Regan et al., 2008) and adds further complications for correlating the deep basin stratigraphy to that on the ridge crest.
- During the late Oligocene to early Miocene, the WAB was marked by a phase of passive infill driven primarily by hemipelagic deposition. We infer that the observed sedimentary signatures are associated with limited tectonism in the basin and scarcity of sediment sources. Our results combined with tectonic models for the Fram Strait region do not support a fully ventilated basin since the late Eocene implied by Poirier and Hillaire-Marcel (2011). However, it is possible that shallow oceanic gateways existed, sustaining an estuarine circulation system. This transitional regime may be reflected by deposition of the Zebra zone sediments from about 36 Ma.
- During the middle Miocene (20–15 Ma), the Amundsen Basin shifted from an isolated basin to an ocean connected to the global meridional ocean circulation system. This change is demarcated by the commencement of sedimentary drift accumulation controlled by geostrophic currents. We infer this depositional phase to be correlative with the condensed late Miocene section in the ACEX borehole of the central LR.

- The two uppermost sedimentary units of likely Plio-Pleistocene age are marked by features controlled by erosion and deposition, such as channels, levees, and scarps, indicative of a high-energy current processes. The modern and buried channel systems are likely generated by dense water masses cascading from the shelf regions north of Greenland. This suggests that brine production by sea-ice freezing may play a bigger role in the Arctic than previously thought.

Acknowledgments
One of the authors (C. F. C.) was supported by a scholarship from the Consejo Nacional de Ciencia y Tecnología (CONACYT) in Mexico. Data acquisition was funded by the Continental Shelf Project of the Kingdom of Denmark. Special thanks to Lars Kjærgaard for his assistance with the loading of multichannel seismic reflection data and GEUS-IT for all their technical support. We thank two anonymous reviewers and Bernard Coakley for constructive reviews of the manuscript that led to substantial revisions and improvements. This paper is published with permission from the Geological Survey of Denmark and Greenland. The LOMROG seismic data presented in this paper are permanently archived at the Geological Survey of Denmark and Greenland (GEUS). Information regarding access to data and databases archived at GEUS is available at https://www.geus.dk. The AWI seismic data are owned and archived by the Alfred Wegener Institute (AWI). Information regarding their data can be obtained from the AWI Geophysics Department (https://www.awi.de/en/science/geosciences/geophysics.html).

References

Assmann, K., Hellmer, H. H., & Beckmann, A. (2003). Seasonal variation in circulation and water mass distribution on the Ross Sea continental shelf. *Antarctic Science*, *15*(1), 3–11. https://doi.org/10.1017/S0954102003001007

Backhaus, J. O., Fohrmann, H., Kämpf, J., & Rubino, A. (1997). Formation and export of water masses produced in Arctic shelf polynyas—Process studies of oceanic convection. *ICES Journal of Marine Science: Journal du Conseil*, *54*(3), 366–382. https://doi.org/10.1006/jmsc.1997.0230

Backman, J., Jakobsson, M., Frank, M., Sangiorgi, F., Brinkhuis, H., Stickley, C., et al. (2008). Age model and core-seismic integration for the Cenozoic Arctic Coring Expedition sediments from the Lomonosov Ridge. *Paleoceanography*, *23*, PA1S03. https://doi.org/10.1029/2007PA001476

Backman, J., Jakobsson, M., Løvlie, R., Polyak, L., & Febo, L. A. (2004). Is the central Arctic Ocean a sediment starved basin? *Quaternary Science Reviews*, *23*(11–13), 1435–1454. https://doi.org/10.1016/j.quascirev.2003.12.005

Backman, J., Moran, K., McInroy, D., & the IODP Expedition 302 Scientists (2005). IODP Expedition 302, Arctic Coring Expedition (ACEX): A first look at the Cenozoic paleoceanography of the Central Arctic Ocean. *Scientific Drilling*, *1*(1, 2005), 12–17. https://doi.org/10.2204/iodp.sd.1.02.2005

Beszczynska-Möller, A., Woodgate, R. A., Lee, C., Melling, H., & Karcher, M. (2011). A synthesis of exchanges through the Main oceanic gateways to the Arctic Ocean. *Oceanography*, *24*(3), 82–99. https://doi.org/10.5670/oceanog.2011.59

Boggild, K., & Mosher, D. (2016). Morphological examination of the NP-28 submarine channel-fan complex in the Amundsen Basin, presented at 42nd Coloquium and Annual Meeting, The Atlantic Geoscience Society (AGS), Nova Scotia, 5–6 February.

Brinkhuis, H., Schouten, S., Collinson, M. E., Sluijs, A., Sinninghe Damsté, J. S., Dickens, G. R., et al. (2006). Episodic fresh surface waters in the Eocene Arctic Ocean. *Nature*, *441*(7093), 606–609. https://doi.org/10.1038/nature04692

Brozena, J. M., Childers, V. A., Lawver, L. A., Gahagan, L. M., Forsberg, R., Faleide, J. I., & Eldholm, O. (2003). New aerogeophysical study of the Eurasia Basin and LR: Implications for basin development. *Geology*, *31*(9), 825–828. https://doi.org/10.1130/g19528.1

Brumley, K., Miller, E. L., Konstantinou, A., Grove, M., Meisling, K. E., & Mayer, L. A. (2015). First bedrock samples dredged from submarine outcrops in the Chukchi Borderland, Arctic Ocean. *Geosphere*, *11*(1), 76–92. https://doi.org/10.1130/GES01044.1s

Bruvoll, V., Kristoffersen, Y., Coakley, B., & Hopper, J. (2010). Hemipelagic deposits on the Mendeleev and northwestern Alpha submarine Ridges in the Arctic Ocean: Acoustic stratigraphy, depositional environment and an inter-ridge correlation calibrated by the ACEX results. *Marine Geophysical Researches*, *31*(3), 149–171. https://doi.org/10.1007/s11001-010-9094-9s

Cande, S. C., & Kent, D. V. (1992). A new magnetic polarity timescale for the Late Cretaceous and Cenozoic. *Journal of Geophysical Research*, *97*, 13,917–13,951. https://doi.org/10.1029/92JB01202s

Cande, S. C., & Kent, D. V. (1995). Revised calibration of the geomagnetic polarity timescale for the late Cretaceous and Cenozoic. *Journal of Geophysical Research, 100*, 6093–6095. https://doi.org/10.1029/94JB03098s

Carmichael, M. J., Lunt, D. J., Huber, M., Heinemann, M., Kiehl, J., LeGrande, A., et al. (2016). A model–model and data–model comparison for the early Eocene hydrological cycle. *Climate of the Past*, *12*(2), 455–481. https://doi.org/10.5194/cp-12-455-2016

Chernykh, A. A., & Krylov, A. A. (2011). Sedimentogenesis in the Amundsen Basin from geophysical data and drilling results on the LR. *Doklady Earth Sciences*, *440*(2), 1372–1376. https://doi.org/10.1134/s1028334x11100011

Chernykh, A. A., & Krylov, A. A. (2017). Duration, causes, and geodynamic significance of the Middle Cenozoic Hiatus in sedimentation in the near-polar part of the LR (based on IODP-302-ACEX drilling data). *Oceanology*, *57*(5), 675–684. https://doi.org/10.1134/S0001437017050058

Chmeleff, J., von Blanckenburg, F., Kossert, K., & Jakob, D. (2010). Determination of the ^{10}Be half-life by multicollector ICP-MS and liquid scintillation counting. *Nuclear Instruments and Methods in Physics Research Section B: Beam Interactions with Materials and Atoms*, *268*(2), 192–199. https://doi.org/10.1016/j.nimb.2009.09.012

Cochran, J. R., Edwards, M. H., & Coakley, B. J. (2006). Morphology and structure of the LR, Arctic Ocean. *Geochemistry, Geophysics, Geosystems*, *7*, Q05019. https://doi.org/10.1029/2005GC001114

Collinson, M. E., Barke, J., van der Burgh, J., van Konijnenburg-van Cittert, J. H. A., Heilmann-Clausen, C., Howard, L. E., & Brinkhuis, H. (2010). Did a single species of Eocene Azolla spread from the Arctic Basin to the southern North Sea? *Review of Palaeobotany and Palynology*, *159*(3–4), 152–165. https://doi.org/10.1016/j.revpalbo.2009.12.001

Dahl-Jensen, T., Larsen, T. B., Woelbern, I., Bach, T., Hanka, W., Kind, R., et al. (2003). Depth to Moho in Greenland: Receiver-function analysis suggests two Proterozoic blocks in Greenland. *Earth and Planetary Science Letters*, *205*(3-4), 379–393. https://doi.org/10.1016/S0012-821X(02)01080-4s

DeMets, C., Gordon, R. G., Argus, D. F., & Stein, S. (1994). Effect of recent revisions to the geomagnetic reversal time scale on estimates of current plate motions. *Geophysical Research Letters*, *21*, 2191–2194. https://doi.org/10.1029/94GL02118

Døssing, A., Hansen, T. M., Olesen, A. V., Hopper, J. R., & Funck, T. (2014). Gravity inversion predicts the nature of the Amundsen Basin and its continental borderlands near Greenland. *Earth and Planetary Science Letters*, *408*, 132–145. https://doi.org/10.1016/j.epsl.2014.10.011

Døssing, A., Hopper, J. R., Olesen, A. V., Rasmussen, T. M., & Halpenny, J. (2013). New aero-gravity results from the Arctic: Linking the latest Cretaceous-early Cenozoic plate kinematics of the North Atlantic and Arctic Ocean. *Geochemistry, Geophysics, Geosystems*, *14*, 4044–4065. https://doi.org/10.1002/ggge.20253

Døssing, A., Jackson, H. R., Matzka, J., Einarsson, I., Rasmussen, T. M., Olesen, A. V., & Brozena, J. M. (2013). On the origin of the Amerasia Basin and the high Arctic large Igneous Province—Results of new aeromagnetic data. *Earth and Planetary Science Letters*, *363*, 219–230. https://doi.org/10.1016/j.epsl.2012.12.013

Engen, Ø., Faleide, J. I., & Dyreng, T. K. (2008). Opening of the Fram Strait gateway: A review of plate tectonic constraints. *Tectonophysics*, *450*(1–4), 51–69. https://doi.org/10.1016/j.tecto.2008.01.002

Faugères, J. C., & Stow, D. A. V. (2008). Chapter 14—Contourite drifts: Nature, evolution and controls. In M. Rebesco & A. Camerlenghi (Eds.), *Developments in sedimentology* (Vol. 60, 1st ed., pp. 257–288). Amsterdam, Netherlands: Elsevier. https://doi.org/10.1016/S0070-4571(08)10014-0

Foldvik, A., & Gammelsrød, T. (1988). Notes on Southern Ocean hydrography, sea-ice and bottom water formation. *Palaeogeography, Palaeoclimatology, Palaeoecology*, *67*(1–2), 3–17. https://doi.org/10.1016/0031-0182(88)90119-8

Föllmi, K. B. (2016). Sedimentary condensation. *Earth-Science Reviews*, *152*(1), 143–180. https://doi.org/10.1016/j.earscirev.2015.11.016

Frank, M., Backman, J., Jakobsson, M., Moran, K., O'Regan, M., King, J., et al. (2008). Beryllium isotopes in Central Arctic Ocean sediments over the past 12.3 million years: Stratigraphic and paleoclimatic implications. *Paleoceanography*, *23*, PA1S02. https://doi.org/10.1029/2007PA001478

Funder, S., Bennike, O., Böcher, J., Israelson, C., Petersen, K. S., & Símonarson, L. A. (2001). *Late Pliocene greenland—The Kap København Formation in North Greenland* (pp. 117–134). Copenhagen: Bulletin of the Geological Society of Denmark.

Fütterer, D. (1992). ARCTIC '91: Die Expedition ARK-VIII/3 Mit FS "Polarstern" 1991 = ARCTIC '91: The expedition ARK-VIII/3 of RV "Polarstern" in 1991, Alfred Wegener Institute for Polar and Marine Research, Bremerhaven.

Gaina, C., Nikishin, A. M., & Petrov, E. I. (2015). Ultraslow spreading, ridge relocation and compressional events in the East Arctic region: A link to the Eurekan orogeny? *Arktos*, *1*(1), 1–11. https://doi.org/10.1007/s41063-015-0006-8

Gales, J. A., Forwick, M., Laberg, J. S., Vorren, T. O., Larter, R. D., Graham, A. G. C., et al. (2013). Arctic and Antarctic submarine gullies—A comparison of high latitude continental margins. *Geomorphology*, *201*, 449–461. https://doi.org/10.1016/j.geomorph.2013.07.018

Geissler, W. H., Jokat, W., & Brekke, H. (2011). The Yermak Plateau in the Arctic Ocean in the light of reflection seismic data—Implication for its tectonic and sedimentary evolution. *Geophysical Journal International*, *187*(3), 1334–1362. https://doi.org/10.1111/j.1365-246X.2011.05197.x

Gill, A. E. (1973). Circulation and bottom water production in the Weddell Sea. *Deep Sea Research and Oceanographic Abstracts*, *20*(2), 111–140. https://doi.org/10.1016/0011-7471(73)90048-X

Gion, A. M., Williams, S. E., & Müller, R. D. (2016). A reconstruction of the Eurekan Orogeny incorporating deformation constraints. *Tectonics*, *36*, 304–320. https://doi.org/10.1002/2015TC004094

Glebovsky, V. Y., Kaminsky, V. D., Minakov, A. N., Merkur'ev, S. A., Childers, V. A., & Brozena, J. M. (2006). Formation of the Eurasia Basin in the Arctic Ocean as inferred from geohistorical analysis of the anomalous magnetic field. *Geotectonics*, *40*(4), 263–281. https://doi.org/10.1134/s0016852106040029

Gong, C., Wang, Y., Hodgson, D. M., Zhu, W., Li, W., Xi, Q., & Li, D. (2014). Origin and anatomy of two different types of mass-transport complexes: A 3D seismic case study from the northern South China Sea margin. *Marine and Petroleum Geology*, *54*, 198–215. https://doi.org/10.1016/j.marpetgeo.2014.03.006

Gregersen, S., Clausen, C., & Dahl-Jensen, T. (1988). Crust and upper mantle structure in Greenland, in Recent Seismological Investigations in Europe, Proceedings of the 19th General Assembly of the ESC, pp. 467–-469, Nauka, Moscow.

Haley, B. A., Frank, M., Spielhagen, R. F., & Eisenhauer, A. (2008). Influence of brine formation on Arctic Ocean circulation over the past 15 million years. *Nature Geoscience*, *1*(1), 68–72. https://doi.org/10.1038/ngeo.2007.5

Heezen, B. C., & Ewing, M. (1961). The Mid-Ocean Ridge and its extension through the Arctic Basin. In G. O. Raasch (Ed.), *Geology of the arctic* (pp. 662–642). Toronto, Canada: University of Toronto Press.

Hernández-Molina, F. J., Llave, E., & Stow, D. A. V. (2008). Chapter 19—Continental slope contourites. In M. Rebesco & A. Camerlenghi (Eds.), *Developments in sedimentology* (pp. 379–408). Oxford: Elsevier Science, Kidlington.

Hopper, J. R., Trinhammer, P., Marcussen, C., & Funck, T. (2012). Acquisition of seismic data in ice filled waters, AGU 2012 Fall Meeting, Abstract C13E-0680.

Howe, J. A., Shimmield, T. M., Harland, R. E. X., & Eyles, N. (2008). Late Quaternary contourites and glaciomarine sedimentation in the Fram Strait. *Sedimentology*. https://doi.org/10.1111/j.1365-3091.2007.00897.x

Jakobsson, M., Backman, J., Rudels, B., Nycander, J., Frank, M., Mayer, L., et al. (2007). The early Miocene onset of a ventilated circulation regime in the Arctic Ocean. *Nature*, *447*(7147), 986–990. https://doi.org/10.1038/nature05924

Jakobsson, M., Mayer, L., Coakley, B., Dowdeswell, J. A., Forbes, S., Fridman, B., et al. (2012). The International Bathymetric Chart of the Arctic Ocean (IBCAO) version 3.0. *Geophysical Research Letters*, *39*, L12609. https://doi.org/10.1029/2012GL052219

Jokat, W. (2005). The sedimentary structure of the LR between 88°N and 80°N. *Geophysical Journal International*, *163*(2), 698–726. https://doi.org/10.1111/j.1365-246X.2005.02786.x

Jokat, W., & Micksch, U. (2004). Sedimentary structure of the Nansen and Amundsen basins, Arctic Ocean. *Geophysical Research Letters*, *31*, L02603. https://doi.org/10.1029/2003GL018352

Jokat, W., Uenzelmann-Neben, G., Kristoffersen, Y., & Rasmussen, T. M. (1992). LR—A double-sided continental margin. *Geology*, *20*(10), 887–890. https://doi.org/10.1130/0091-7613(1992)020<0887:lradsc>2.3.co

Jokat, W., Weigelt, E., Kristoffersen, Y., Rasmussen, T., & Schöone, T. (1995a). New insights into the evolution of the Lomonosov Ridge and the Eurasian Basin. *Geophysical Journal International*, *122*(2), 378–392. https://doi.org/10.1111/j.1365-246X.1995.tb00532.x

Jokat, W., Weigelt, E., Kristoffersen, Y., Rasmussen, T., & Schöone, T. (1995b). New geophysical results from the south-western Eurasian Basin (Morris Jesup Rise, Gakkel Ridge, Yermak Plateau) and the Fram Strait. *Geophysical Journal International*, *123*(2), 601–610. https://doi.org/10.1111/j.1365-246X.1995.tb06874.x

Jones, E. P., Rudels, B., & Anderson, L. G. (1995). Deep waters of the Arctic Ocean: Origins and circulation. *Deep-Sea Research Part I: Oceanographic Research Papers*, *42*(5), 737–760. https://doi.org/10.1016/0967-0637(95)0013-V

Klaucke, I., Hesse, R., & Ryan, W. B. F. (1998). Seismic stratigraphy of the Northwest Atlantic Mid-Ocean Channel: Growth pattern of a mid-ocean channel-levee complex. *Marine and Petroleum Geology*, *15*(6), 575–585. https://doi.org/10.1016/S0264-8172(98)00044-0

Kneller, B., & Buckee, C. (2000). The structure and fluid mechanics of turbidity currents: A review of some recent studies and their geological implications. *Sedimentology*, *47*, 62–94. https://doi.org/10.1046/j.1365-3091.2000.047s1062.x

Knudsen, C, Hopper, J. R., Bierman, P. R., Bjerager, M., Funck, T., Ineson, J., et al. (2017). Samples from the Lomonosov Ridge place new constraints on the geological evolution of the Arctic Ocean. In V. Pease & B. J. Coakley (Eds.) *Circum-Arctic lithosphere evolution*, *Geological Society, Special Publications, London*, *460*, 397–418. https://doi.org/10.1144/SP460.17

Knutz, P. C., Hopper, J. R., Gregersen, U., Nielsen, T., & Japsen, P. (2015). A contourite drift system on the Baffin Bay–West Greenland margin linking Pliocene Arctic warming to poleward ocean circulation. *Geology*, *43*(10), 907–910. https://doi.org/10.1130/g36927.1

Kristoffersen, Y., Sorokin, M. Y., Jokat, W., & Svendsen, O. (2004). A submarine fan in the Amundsen Basin, Arctic Ocean. *Marine Geology*, *204*(3–4), 317–324. https://doi.org/10.1016/S0025-3227(03)00373-6

Kusahara, K., Hasumi, H., & Williams, G. D. (2011). Dense shelf water formation and brine-driven circulation in the Adélie and George V Land region. *Ocean Modelling*, *37*(3–4), 122–138. https://doi.org/10.1016/j.ocemod.2011.01.008

Lindsay, R., & Schweiger, A. (2015). Arctic sea ice thickness loss determined using subsurface, aircraft, and satellite observations. *The Cryosphere*, *9*(1), 269–283. https://doi.org/10.5194/tc-9-269-2015

Lykke-Andersen, H., Funck, T., Hopper, J.R., Trinhammer, P., Marcussen, C., Gunvald, A. K., & Jørgensen, E. V. (2010). Seismic Acquisition Report - LOMROG 2009. Danmarks and Grønlands Geologiske Undersøgelse Rapport, 2010/53, 73pp. (excl. appendices).

Mann, U., Knies, J., Chand, S., Jokat, W., Stein, R., & Zweigel, J. (2009). Evaluation and modelling of Tertiary source rocks in the central Arctic Ocean. *Marine and Petroleum Geology*, *26*(8), 1624–1639. https://doi.org/10.1016/j.marpetgeo.2009.01.008

Marcussen, C., Vangkilde-Pedersen, T., Lykke-Andersen, H., Trinhammer, P., Funck, T., Dahl-Jensen, T., & Forsberg, R. (2008). Seismic Acquisition Report - LOMROG 2007. Danmarks and Grønlands Geologiske Undersøgelse Rapport 2008/77, 82 pp (excl. appendices).

Marsland, S. J., Bindoff, N. L., Williams, G. D., & Budd, W. F. (2004). Modeling water mass formation in the Mertz Glacier Polynya and Adélie Depression, East Antarctica. *Journal of Geophysical Research*, *109*, C11003. https://doi.org/10.1029/2004JC002441

März, C., Vogt, C., Schnetger, B., & Brumsack, H. -J. (2011). Variable Eocene-Miocene sedimentation processes and bottom water redox conditions in the Central Arctic Ocean (IODP expedition 302). *Earth and Planetary Science Letters*, *310*(3-4), 526–537. https://doi.org/10.1016/j.epsl. 2011.08.025s

Mattingsdal, R., Knies, J., Andreassen, K., Fabian, K., Husum, K., Grøsfjeld, K., & De Schepper, S. (2014). A new 6 Myr stratigraphic framework for the Atlantic–Arctic gateway. *Quaternary Science Reviews*, *92*, 170–178. https://doi.org/10.1016/j.quascirev.2013.08.022

Mauritzen, C. (1996). Production of dense overflow waters feeding the North Atlantic across the Greenland-Scotland Ridge. Part 1: Evidence for a revised circulation scheme. *Deep Sea Research Part I: Oceanographic Research Papers*, *43*(6), 769–806. https://doi.org/10.1016/0967-0637(96)00037-4

McCave, I. N., & Hall, I. R. (2006). Size sorting in marine muds: Processes, pitfalls, and prospects for paleoflow-speed proxies. *Geochemistry, Geophysics, Geosystems*, *7*, Q10N05. https://doi.org/10.1029/2006GC001284

McKenzie, D. (1978). Some remarks on the development of sedimentary basins. *Earth and Planetary Science Letters*, *40*(1), 25–32. https://doi.org/10.1016/0012-821X(78)90071-7

Menard, H. W. (1955). Deep-sea channels, topography, and sedimentation. *AAPG Bulletin*, *39*(2), 236–255.

Michael, P. J., Langmuir, C. H., Dick, H. J. B., Snow, J. E., Goldstein, S. L., Graham, D. W., et al. (2003). Magmatic and amagmatic seafloor generation at the ultraslow-spreading Gakkel ridge, Arctic Ocean. *Nature*, *423*(6943), 956–961. https://doi.org/10.1038/nature01704

Minakov, A. N., & Podladchikov, Y. Y. (2012). Tectonic subsidence of the Lomonosov Ridge. *Geology*, *40*(2), 99–102. https://doi.org/10.1130/g32445.1

Mitchum, R. M. Jr., Vail, P. R., & Sangree, J. B. (1977). Seismic stratigraphy and global changes of sea level, part 6: Stratigraphic interpretation of seismic reflection patterns in depositional sequences. In C. Paynton (Ed.), *Seismic stratigraphy—Applications to hydrocarbon exploration* (pp. 117–133). Tulsa: AAPG Memoir.

Moore, T. C., & the Expedition 302 Scientists (2006a). Sedimentation and subsidence history of the LR. In J. Backman, K. Moran, D. B. McInroy, L. A. Mayer, and the Expedition 302 Scientist *Proc. IODP*, 302: Edinburgh (Integrated Ocean Drilling Program Management International, Inc.). https://doi.org/10.2204/iodp.proc.302.105.2006

Moore, T. C., & the Expedition 302 Scientists (2006b). Sites M0001 – M0004. In J. Backman, K. Moran, D. B. McInroy, L. A. Mayer, and the Expedition 302 Scientist *Proc. IODP*, 302: Edinburgh (Integrated Ocean Drilling Program Management International, Inc.). https://doi.org/10.2204/iodp.proc.302.104.2006

Moran, K., Backman, J., Brinkhuis, H., Clemens, S. C., Cronin, T., Dickens, G. R., et al. (2006). The Cenozoic palaeoenvironment of the Arctic Ocean. *Nature*, *441*(7093), 601–605. https://doi.org/10.1038/nature04800

Mulder, T., & Syvitski, J. P. M. (1995). Turbidity currents generated at river mouths during exceptional discharges to the world oceans. *The Journal of Geology*, *103*(3), 285–299. https://doi.org/10.1086/629747

Oakey, G. N., & Chalmers, J. A. (2012). A new model for the Paleogene motion of Greenland relative to North America: Plate reconstructions of the Davis Strait and Nares Strait regions between Canada and Greenland. *Journal of Geophysical Research*, *117*, B10401. https://doi.org/10.1029/2011JB008942

Oakey, G. N., & Stephenson, R. (2008). Crustal structure of the Innuitian region of Arctic Canada and Greenland from gravity modelling: Implications for the Palaeogene Eurekan orogen. *Geophysical Journal International*, *173*(3), 1039–1063. https://doi.org/10.1111/j.1365-246X.2008.03784.x

Ogg, J. G. (2012). Chapter 5—Geomagnetic polarity time scale. In F. M. Gradstein, J. G. Ogg, M. D. Schmitz, & G. M. Ogg (Eds.), *The geologic time scale* (pp. 85–113). Boston: Elsevier. https://doi.org/10.1016/B978-0-444-59425-9.00005-6

Ohshima, K. I., Fukamachi, Y., Williams, G. D., Nihashi, S., Roquet, F., Kitade, Y., et al. (2013). Antarctic bottom water production by intense sea-ice formation in the Cape Darnley polynya. *Nature Geoscience*, *6*(3), 235–240. https://doi.org/10.1038/ngeo1738

O'Regan, M., Moran, K., Backman, J., Jakobsson, M., Sangiorgi, F., Brinkhuis, H., et al. (2008). Mid-Cenozoic tectonic and paleoenvironmental setting of the central Arctic Ocean. *Paleoceanography*, *23*, PA1S20. https://doi.org/10.1029/2007PA001559

O'Regan, M., Moran, K., Baxter, C. D. P., Cartwright, J., Vogt, C., & Kölling, M. (2010). Towards ground truthing exploration in the central Arctic Ocean: A Cenozoic compaction history from the LR. *Basin Research*, *22*(2), 215–235. https://doi.org/10.1111/j.1365-2117.2009.00403.x

O'Regan, M., Williams, C. J., Frey, K. E., & Jakobsson, M. (2011). A synthesis of the long-term paleoclimatic evolution of the Arctic. *Oceanography*, *24*(3), 66–80. https://doi.org/10.5670/oceanog.2011.57

Ostenso, N. A., & Wold, R. J. (1977). A seismic and gravity profile across the Arctic Ocean Basin. *Tectonophysics*, *37*(1–3), 1–1), 24. https://doi.org/10.1016/0040-1951(77)90036-1

Pagani, M., Pedentchouk, N., Huber, M., Sluijs, A., Schouten, S., Brinkhuis, H., et al., & the Expedition 302 Scientists (2006). Arctic hydrology during global warming at the Palaeocene/Eocene thermal maximum. *Nature*, *442*(7103), 671–675. https://doi.org/10.1038/nature05043

Parker, G. (1982). Conditions for the ignition of catastrophically erosive turbidity currents. *Marine Geology*, *46*(3–4), 307–327. https://doi.org/10.1016/0025-3227(82)90086-X

Parsons, B., & Sclater, J. G. (1977). An analysis of the variation of ocean floor bathymetry and heat flow with age. *Journal of Geophysical Research*, *82*, 803–827. https://doi.org/10.1029/JB082i005p00803

Pickering, K. T., Clark, J. D., Smith, R. D. A., Hiscott, R. N., Ricci Lucchi, F., & Kenyon, N. H. (1995). Architectural element analysis of turbidite systems, and selected topical problems for sand-prone deep-water systems. In K. T. Pickering, R. N. Hiscott, N. H. Kenyon, F. Ricci Lucchi, & R. D. A. Smith (Eds.), *Atlas of deep water environments: Architectural style in turbidite systems* (pp. 1–10). Dordrecht: Springer Netherlands. https://doi.org/10.1007/978-94-011-1234-5_1

Piepjohn, K., von Gosen, W., & Tessensohn, F. (2016). The Eurekan deformation in the Arctic: An outline. *Journal of the Geological Society*, *173*(6), 1007–1024. https://doi.org/10.1144/jgs2016-081

Piper, D. J. W., Deptuck, M. E., Mosher, D. C., Clarke, J. E. H., & Migeon, S. (2012). Erosional and depositional features of glacial meltwater discharges on the eastern Canadian continental margin. In B. E. Prather, M. E. Deptuck, D. Mohring, B. V. Hoorn, & R. B. Wynn (Eds.), *Application of the principles of seismic geomorphology to continental slope and base-of-slope systems* (pp. 61–80). Tulsa, OK: SEPM Society for Sedimentary Geology. https://doi.org/10.2110/pec.12.99.0061

Poirier, A., & Hillaire-Marcel, C. (2009). Os-isotope insights into major environmental changes of the Arctic Ocean during the Cenozoic. *Geophysical Research Letters*, *36*, L11602. https://doi.org/10.1029/2009GL037422

Poirier, A., & Hillaire-Marcel, C. (2011). Improved Os-isotope stratigraphy of the Arctic Ocean. *Geophysical Research Letters*, *38*, L14607. https://doi.org/10.1029/2011GL047953

Poselov, V., Butsenki, V., Chernykh, A., Glebovsky, V., Jackson, H. R., Potter, D. P., et al. (2014). The structural integrity of the LR withhe North American and Siberian continental margins, paper presented at International Conference on Arctic Margins VI, Fairbanks, Alaska, May 2011.

Presti, M., De Santis, L., Busetti, M., & Harris, P. T. (2003). Late Pleistocene and Holocene sedimentation on the George V Continental Shelf, East Antarctica. *Deep Sea Research Part II: Topical Studies in Oceanography*, *50*(8–9), 1441–1461. https://doi.org/10.1016/S0967-0645(03)00068-7

Rashid, H., Hesse, R., & Piper, D. J. W. (2003). Origin of unusually thick Heinrich layers in ice-proximal regions of the northwest Labrador Sea. *Earth and Planetary Science Letters*, *208*(3–4), 319–336. https://doi.org/10.1016/S0012-821X(03)00030-X

Rebesco, M., Hernández-Molina, F. J., Van Rooij, D., & Wåhlin, A. (2014). Contourites and associated sediments controlled by deep-water circulation processes: State-of-the-art and future considerations. *Marine Geology*, *352*, 111–154. https://doi.org/10.1016/j.margeo.2014.03.011

Rebesco, M., Wåhlin, A., Laberg, J. S., Schauer, U., Beszczynska-Möller, A., Lucchi, R. G., et al. (2013). Quaternary contourite drifts of the Western Spitsbergen margin. *Deep Sea Research Part I: Oceanographic Research Papers*, *79*, 156–168. https://doi.org/10.1016/j.dsr.2013.05.013

Ritzmann, O., Jokat, W., Czuba, W., Guterch, A., Mjelde, R., & Nishimura, Y. (2004). A deep seismic transect from Hovgård Ridge to northwestern Svalbard across the continental-ocean transition: A sheared margin study. *Geophysical Journal International*, *157*(2), 683–702. https://doi.org/10.1111/j.1365-246X.2004.02204.xs

Rudels, B. (1995). The thermohaline circulation of the Arctic Ocean and the Greenland Sea. *Philosophical Transactions: Physical Sciences and Engineering*, *352*(1699), 287–299.

Rudels, B. (2012). Arctic Ocean circulation and variability—Advection and external forcing encounter constraints and local processes. *Ocean Science*, *8*(2), 261–286. https://doi.org/10.5194/os-8-261-2012

Rudels, B., Fahrbach, E., Meincke, J., Budéus, G., & Eriksson, P. (2002). The East Greenland current and its contribution to the Denmark Strait overflow. *ICES Journal of Marine Science*, *59*(6), 1133–1154. https://doi.org/10.1006/jmsc.2002.1284

Rudels, B., & Friedrich, H. (2000). The transformations of Atlantic water in the Arctic Ocean and their significance for the freshwater budget. In L. L. Lewis, E. P. Jones, P. Lemke, T. D. Prowse, & P. Wadhams (Eds.), *The freshwater budget of the Arctic Ocean* (pp. 503–532). The Netherlands: Kluwer Academic Publishers.

Russell, S. M. (1999). A magnetic study of the West Iberia and conjugate rifted continental margins: Constraints on rift-to-drift process, (PhD Thesis) (278 pp.). UK: University of Durham.

Sangiorgi, F., Brumsack, H.-J., Willard, D. A., Schouten, S., Stickley, C. E., O'Regan, M., et al. (2008). A 26 million year gap in the Central Arctic record at the greenhouse-icehouse transition: Looking for clues. *Paleoceanography*, *23*, PA1S04. https://doi.org/10.1029/2007PA001477

Serreze, M. C., & Barry, R. G. (2005). Arctic Ocean–sea ice–climate interactions. In *The Arctic climate system* (pp. 177–207). Cambridge: Cambridge University Press. https://doi.org/10.1017/CBO9780511535888.008

Smith, J. A., Hillenbrand, C.-D., Pudsey, C. J., Allen, C. S., & Graham, A. G. C. (2010). The presence of polynyas in the Weddell Sea during the last glacial period with implications for the reconstruction of sea-ice limits and ice sheet history. *Earth and Planetary Science Letters*, *296*(3–4), 287–298. https://doi.org/10.1016/j.epsl.2010.05.008

Speelman, E. N., Van Kempen, M. M. L., Barke, J., Brinkhuis, H., Reichart, G. J., Smolders, A. J. P., et al. (2009). The Eocene Arctic Azolla bloom: Environmental conditions, productivity and carbon drawdown. *Geobiology*, *7*(2), 155–170. https://doi.org/10.1111/j.1472-4669.2009.00195.x

St. John, K. (2008). Cenozoic ice-rafting history of the central Arctic Ocean: Terrigenous sands on the LR. *Paleoceanography*, *23*, PA1S05. https://doi.org/10.1029/2007PA001483

Stein, R., Boucsein, B., & Meyer, H. (2006). Anoxia and high primary production in the Paleogene central Arctic Ocean: First detailed records from LR. *Geophysical Research Letters*, *33*, L18606. https://doi.org/10.1029/2006GL026776

Stein, R., Fahl, K., Schreck, M., Knorr, G., Niessen, F., Forwick, M., et al. (2016). Evidence for ice-free summers in the late Miocene central Arctic Ocean. *Nature Communications*, *7*, 11148. https://doi.org/10.1038/ncomms11148

Stein, R., Weller, P., Backman, J., Brinkhuis, H., Moran, K., & Pälike, H. (2014). Chapter 3.2 - Cenozoic Arctic Ocean climate history: Some highlights from the Integrated Ocean Drilling Program Arctic Coring Expedition. In R. Stein, D. Blackman, F. Inagaki, & H.-C. Larsen (Eds.), *Developments in Marine Geology* (Vol. 7, 1st ed., pp. 259–293). Amsterdam, Netherlands: Elsevier. https://doi.org/10.1016/B978-0-444-62617-2.00011-6

Stickley, C. E., St John, K., Koç, N., Jordan, R. W., Passchier, S., Pearce, R. B., & Kearns, L. E. (2009). Evidence for middle Eocene Arctic sea ice from diatoms and ice-rafted debris. *Nature*, *460*(7253), 376–379. https://doi.org/10.1038/nature08163

Svindland, K. T., & Vorren, T. O. (2002). Late Cenozoic sedimentary environments in the Amundsen Basin, Arctic Ocean. *Marine Geology*, *186*(3–4), 541–555. https://doi.org/10.1016/S0025-3227(02)00197-4

Sweeney, J. F., Weber, J. R., & Blasco, S. M. (1982). Structure of the Arctic continental ridges in the Arctic Ocean: Lorex constraints. *Tectonophysics*, *89*(1-3), 217–237. https://doi.org/10.1016/0040-1951(82)90039-7

Talwani, M., & Eldholm, O. (1977). Evolution of the Norwegian-Greenland Sea. *Geological Society of America Bulletin*, *88*(7), 969–999. https://doi.org/10.1130/0016-7606(1977)88<969:eotns>2.0.co;2

Tomczak, M., & Godfrey, J. S. (1994). Chapter 7—Arctic oceanography; the path of North Atlantic Deep Water. In M. Tomczak & J. S. Godfrey (Eds.), *Regional oceanography* (pp. 89–111). Amsterdam: Pergamon. https://doi.org/10.1016/B978-0-08-041021-0.50011-4

van der Burgh, J., Collinson, M. E., van Konijnenburg-van Cittert, J. H. A., Barke, J., & Brinkhuis, H. (2013). The freshwater fern Azolla (Azollaceae) from Eocene Arctic and Nordic Sea sediments: New species and their stratigraphic distribution. *Review of Palaeobotany and Palynology*, *194*, 50–68. https://doi.org/10.1016/j.revpalbo.2013.02.002

Varming, T., Funck, T., Hopper, J.R., Trinhammer, P., Ejlertsen, S., Rödel, L., et al. 2012. Seismic Acquisition Report - LOMROG 2012. Danmarks and Grønlands Geologiske Undersøgelse Rapport 2012/120, 77pp (excl. appendices).

Vogt, P. R., Taylor, P. T., Kovacs, L. C., & Johnson, G. L. (1979). Detailed aeromagnetic investigation of the Arctic Basin. *Journal of Geophysical Research*, *84*, 1071–1089. https://doi.org/10.1029/JB084iB03p01071

Weigelt, E., Jokat, W., & Franke, D. (2014). Seismostratigraphy of the Siberian Sector of the Arctic Ocean and adjacent Laptev Sea Shelf. *Journal of Geophysical Research: Solid Earth*, *119*, 5275–5289. https://doi.org/10.1002/2013jb010727

Wold, C. N. (1994). Cenozoic sediment accumulation on drifts in the northern North Atlantic. *Paleoceanography*, *9*, 917–941. https://doi.org/10.1029/94PA01438

Wolf-Welling, T. C. W., Cremer, M., O'Connell, S., Winkler, A., & Thiede, J. (1996). Cenozoic Arctic gateway paleoclimate variability: Indications from changes in coarse-fraction composition, in Proceedings of the Ocean Drilling Program, 151 *Scientific Results*, International Ocean Discovery Program (IODP). https://doi.org/10.2973/odp.proc.sr.151.139.1996

Woodgate, R. (2013). Arctic Ocean circulation: Going around at the top of the world. *Nature Education Knowledge*, *4*(8), 8.

Zachos, J. C., Dickens, G. R., & Zeebe, R. E. (2008). An early Cenozoic perspective on greenhouse warming and carbon-cycle dynamics. *Nature*, *451*(7176), 279–283. https://doi.org/10.1038/nature06588

Zachos, J. C., Pagani, M., Sloan, L., Thomas, E., & Billups, K. (2001). Trends, rhythms, and aberrations in global climate 65 Ma to present. *Science*, *292*(5517), 686–693. https://doi.org/10.1126/science.1059412

Zelt, C. A., & Smith, R. B. (1992). Seismic traveltime inversion for 2-D crustal velocity structure. *Geophysical Journal International*, *108*(1), 16–34. https://doi.org/10.1111/j.1365-246X.1992.tb00836.xs